Published by Institute of Physics Publishing for SISSA

Received: *November 30, 2007*
Accepted: *November 30, 2007*
Published: *December 27, 2007*

NNLO corrections to event shapes in e^+e^- annihilation

A. Gehrmann-De Ridder

Institute for Theoretical Physics, ETH, CH-8093 Zürich, Switzerland
E-mail: gehra@phys.ethz.ch

T. Gehrmann

Institut für Theoretische Physik, Universität Zürich,
Winterthurerstrasse 190, CH-8057 Zürich, Switzerland
E-mail: thomas.gehrmann@physik.unizh.ch

E.W.N. Glover

Institute of Particle Physics Phenomenology, Department of Physics,
University of Durham, Durham, DH1 3LE, U.K.
E-mail: e.w.n.glover@durham.ac.uk

G. Heinrich

School of Physics, The University of Edinburgh,
Edinburgh EH9 3JZ, U.K.
E-mail: gheinric@ph.ed.ac.uk

Abstract: We compute the next-to-next-to-leading order (NNLO) QCD corrections to the six most important event shape variables related to three-particle final states in electron-positron annihilation. The corrections are sizeable for all variables, however their magnitude is substantially different for different observables. We observe that the NNLO corrections yield a considerably better agreement between theory and experimental data both in shape and normalisation of the event shape distributions. The renormalisation scale dependence of the theoretical prediction is substantially reduced compared to the previously existing NLO results. Our results will allow a precise determination of the strong coupling constant from event shape data collected at LEP.

Keywords: QCD, Jets, NLO Computations, LEP HERA and SLC Physics.

Contents

1. Introduction **1**

2. Event shape variables **2**

3. Event shapes in perturbation theory **5**

4. Calculation of NNLO corrections **7**

5. NNLO distributions **9**
- 5.1 Thrust 10
- 5.2 Heavy jet mass 11
- 5.3 Jet broadenings 12
- 5.4 C-parameter 13
- 5.5 Y_3 13

6. Comparison with data **14**
- 6.1 Thrust 14
- 6.2 Heavy jet mass 15
- 6.3 Jet broadenings 17
- 6.4 C-parameter 21
- 6.5 Y_3 22

7. Conclusions and outlook **24**

JHEP12(2007)094

1. Introduction

For more than a decade experiments at LEP (CERN) and SLC (SLAC) gathered a wealth of high precision high energy hadronic data from electron-positron annihilation at a range of centre-of-mass energies [1 – 5]. This data provides one of the cleanest ways of probing our quantitative understanding of QCD. This is particularly so because the strong interactions occur only in the final state and are not entangled with the parton density functions associated with beams of hadrons. As the understanding of the strong interaction, and the capability of making more precise theoretical predictions, develops, more and more stringent comparisons of theory and experiment are possible, leading to improved measurements of fundamental quantities such as the strong coupling constant [6].

In addition to measuring multi-jet production rates, more specific information about the topology of the events can be extracted. To this end, many variables have been introduced which characterise the hadronic structure of an event. For example, we can ask

how planar or how collimated an event is. In general, a variable is described as n jet-like if it vanishes for a final state configuration of $(n-1)$ hadrons[1]. With the precision data from LEP and SLC, experimental distributions for such event shape variables have been extensively studied and have been compared with theoretical calculations based on next-to-leading order (NLO) parton-level event generator programs [7 – 9], improved by resumming kinematically-dominant leading and next-to-leading logarithms (NLO+NLL) [10, 11] and by the inclusion of non-perturbative models of power-suppressed hadronisation effects [12].

Comparing the different sources of error in the extraction of α_s from hadronic data, one finds that the purely experimental error is negligible compared to the theoretical uncertainty. There are two sources of theoretical uncertainty: the theoretical description of the parton-to-hadron transition (hadronisation uncertainty) and the uncertainty stemming from the truncation of the perturbative series at a certain order, as estimated by scale variations (perturbative or scale uncertainty). Although the precise size of the hadronisation uncertainty is debatable and perhaps often underestimated, it is conventional to consider the scale uncertainty as the dominant source of theoretical error on the precise determination of α_s from three-jet observables.

For the bulk of the paper we are concerned with the next-to-next-to-leading order (NNLO) perturbative corrections to three jet-like shape variables. To be precise, we present the NNLO coefficients for the differential distributions of thrust, the wide and total jet broadening, heavy hemisphere mass, C parameter and the jet transition variable Y_3 for the Durham jet algorithm. These results are obtained using a numerical implementation of the two-loop $\gamma^* \to 3$ parton [13], the one-loop $\gamma^* \to 4$ partons [14] and the tree-level $\gamma^* \to 5$ parton matrix elements [15]. Each of the contributions becomes singular when one or more partons are soft and/or collinear. In previous work, we have developed an antenna subtraction method [16] for isolating singularities and ensuring that the final result is infrared finite [17]. The resulting numerical program, `EERAD3`, yields the full kinematical information on the partonic final state and can be applied to generic infrared safe three-jet observables.

In section 2, we provide definitions of the relevant three-jet shape variables while section 3 reviews the structure of the perturbative predictions. Section 4 gives a brief description of the NNLO calculation and its implementation in the multi-purpose parton level Monte Carlo program `EERAD3`. Results for the event shape distributions are reported in sections 5 and 6, together with an estimate of the remaining perturbative uncertainty due to variations of the renormalisation scale. The parton level predictions are also compared with hadron-level experimental data. Finally, our results are summarised in section 7.

2. Event shape variables

In order to characterise hadronic final states in electron-positron annihilation, a variety of event shape variables have been proposed in the literature, for a review see e.g. [18].

[1]It should be noted that sometimes in the literature, especially in works on resummation, event shapes requiring three particles are called two-jet event shapes, while those requiring four particles are called three-jet event shapes.

JHEP12(2007)094

These variables can be categorised into two classes, according to the minimal number of final-state particles required for them to be non-vanishing: the most common variables require three particles (and are thus closely related to three-jet final states), while several other variables were constructed such that they require at least four particles (related to four-jet final states).

Among the event shapes requiring three-particle final states, six variables were studied in great detail: the thrust T [19], the normalised heavy jet mass M_H^2/s [20], the wide and total jet broadenings B_W and B_T [21], the C-parameter [22] and the transition from three-jet to two-jet final states in the Durham jet algorithm Y_3 [23].

(a) Thrust, T [19].

The thrust variable for a hadronic final state in e^+e^- annihilation is defined as [19]

$$T = \max_{\vec{n}} \left(\frac{\sum_i |\vec{p}_i \cdot \vec{n}|}{\sum_i |\vec{p}_i|} \right) , \tag{2.1}$$

where $\vec{p}_i$ denotes the three-momentum of particle i, with the sum running over all particles. The unit vector $\vec{n}$ is varied to find the thrust direction $\vec{n}_T$ which maximises the expression in parentheses.

The maximum value of thrust, $T \to 1$, is obtained in the limit where there are only two particles in the event. For a three-particle event the minimum value of thrust is $T = 2/3$.

(b) Heavy hemisphere mass, M_H^2/s [20].

In the original definition [20] one divides the event into two hemispheres. In each hemisphere, H_i, one also computes the hemisphere invariant mass as:

$$M_i^2/s = \frac{1}{E_{\rm vis}^2} \left(\sum_{k \in H_i} p_k \right)^2 , \tag{2.2}$$

where $E_{\rm vis}$ is the total energy visible in the event. In the original definition, the hemisphere is chosen such that $M_1^2 + M_2^2$ is minimised. We follow the more customary definition whereby the hemispheres are separated by the plane orthogonal to the thrust axis.

The larger of the two hemisphere invariant masses yields the heavy jet mass:

$$\rho \equiv M_H^2/s = \max(M_1^2/s, M_2^2/s) . \tag{2.3}$$

In the two-particle limit $\rho \to 0$, while for a three-particle event $\rho \leq 1/3$.

The associated light hemisphere mass,

$$M_L^2/s = \min(M_1^2/s, M_2^2/s) \tag{2.4}$$

is an example of a four-jet observable and vanishes in the three-particle limit.

At lowest order, the heavy jet mass and the $(1 - T)$ distribution are identical. However, this degeneracy is lifted at next-to-leading order.

(c) Jet Broadening, B_W and B_T [21].

Taking a plane perpendicular to $\vec{n}_T$ through the coordinate origin, one defines two event hemispheres $H_{1,2}$. In each of them, one determines the hemisphere broadening:

$$B_i = \frac{\sum_{k \in H_i} |\vec{p_k} \times \vec{n}_T|}{2 \sum_k |\vec{p_k}|} . \tag{2.5}$$

The wide and total jet broadening are then defined as

$$B_W = \max(B_1, B_2) , \tag{2.6}$$

$$B_T = B_1 + B_2 . \tag{2.7}$$

In the two-particle limit $B_W \to 0$ and $B_T \to 0$. The maximum broadening for a three-particle event is $B_T = B_W = 1/(2\sqrt{3})$.

The narrow jet broadening,

$$B_N = \min(B_1, B_2) , \tag{2.8}$$

is another four-jet observable and vanishes when only three particles are in the event.

(d) The C parameter, [22].

The linearised momentum tensor

$$\Theta^{\alpha\beta} = \frac{1}{\sum_k |\vec{p_k}|} \sum_k \frac{p_k^\alpha p_k^\beta}{|\vec{p_k}|} , \qquad (\alpha, \beta = 1, 2, 3) , \tag{2.9}$$

has three eigenvalues λ_i, which are used to construct the C-parameter:

$$C = 3 \left(\lambda_1\lambda_2 + \lambda_2\lambda_3 + \lambda_3\lambda_1\right) . \tag{2.10}$$

This definition is equivalent to

$$C = 3 \left(\Theta^{11}\Theta^{22} + \Theta^{22}\Theta^{33} + \Theta^{33}\Theta^{11} - \Theta^{12}\Theta^{12} - \Theta^{23}\Theta^{23} - \Theta^{31}\Theta^{31}\right) . \tag{2.11}$$

The related four-jet observable is the D-parameter,

$$D = 27\, \lambda_1\lambda_2\lambda_3 . \tag{2.12}$$

(e) The jet transition variable, Y_3 [23].

The jet transition variable Y_3 is defined as the value of the jet resolution parameter $y_{\rm cut}$ for which an event changes from a three-jet to a two-jet configuration with some jet defining scheme.

Here, we focus on the Durham jet algorithm which clusters particles into jets by computing the measurement variable

$$y_{ij,D} = \frac{2\min(E_i^2, E_j^2)(1-\cos\theta_{ij})}{E_{\rm vis}^2} \tag{2.13}$$

for each pair (i, j) of particles. The pair with the lowest $y_{ij,D}$ is replaced by a pseudoparticle whose four-momentum is given by the sum of the four-momenta of particles i and j ('E' recombination scheme). This procedure is repeated as long as pairs with invariant mass below the predefined resolution parameter $y_{ij,D} < y_{\rm cut}$ are found. Once the clustering is terminated, the remaining (pseudo-)particles are the jets.

3. Event shapes in perturbation theory

The perturbative expansion for the distribution of a generic observable y up to NNLO at centre-of-mass energy $\sqrt{s}$ for renormalisation scale $\mu^2 = s$ and $\alpha_s \equiv \alpha_s(\sqrt{s})$ is given by

$$\frac{1}{\sigma_{\rm had}}\frac{{\rm d}\sigma}{{\rm d}y} = \left(\frac{\alpha_s}{2\pi}\right)\frac{{\rm d}\bar{A}}{{\rm d}y} + \left(\frac{\alpha_s}{2\pi}\right)^2\frac{{\rm d}\bar{B}}{{\rm d}y} + \left(\frac{\alpha_s}{2\pi}\right)^3\frac{{\rm d}\bar{C}}{{\rm d}y} + \mathcal{O}(\alpha_s^4)\,. \tag{3.1}$$

Here the event shape distribution is normalised to the total hadronic cross section $\sigma_{\rm had}$. With the assumption of massless quarks, then at NNLO we have,

$$\sigma_{\rm had} = \sigma_0\left(1 + \frac{3}{2}C_F\left(\frac{\alpha_s}{2\pi}\right) + K_2\left(\frac{\alpha_s}{2\pi}\right)^2 + \mathcal{O}(\alpha_s^3)\right)\,, \tag{3.2}$$

where the Born cross section for $e^+e^- \to q\bar{q}$ is

$$\sigma_0 = \frac{4\pi\alpha}{3s}N\,e_q^2\,. \tag{3.3}$$

The constant K_2 is given by,

$$K_2 = \frac{1}{4}\left[-\frac{3}{2}C_F^2 + C_F C_A\left(\frac{123}{2} - 44\zeta_3\right) + C_F T_R N_F\left(-22 + 16\zeta_3\right)\right]\,, \tag{3.4}$$

where the QCD colour factors are

$$C_A = N, \qquad C_F = \frac{N^2-1}{2N}, \qquad T_R = \frac{1}{2} \tag{3.5}$$

for $N = 3$ colours and N_F light quark flavours.

In practice, we compute the perturbative coefficients A, B and C, which are all normalised to σ_0:

$$\frac{1}{\sigma_0}\frac{{\rm d}\sigma}{dy} = \left(\frac{\alpha_s}{2\pi}\right)\frac{{\rm d}A}{{\rm d}y} + \left(\frac{\alpha_s}{2\pi}\right)^2\frac{{\rm d}B}{{\rm d}y} + \left(\frac{\alpha_s}{2\pi}\right)^3\frac{{\rm d}C}{{\rm d}y} + \mathcal{O}(\alpha_s^4)\,. \tag{3.6}$$

However, A, B and C are straightforwardly related to $\bar{A}$, $\bar{B}$ and $\bar{C}$,

$$\begin{aligned}\bar{A} &= A\,,\\ \bar{B} &= B - \frac{3}{2}C_F\,A\,,\\ \bar{C} &= C - \frac{3}{2}C_F\,B + \left(\frac{9}{4}C_F^2 - K_2\right)A\,.\end{aligned} \tag{3.7}$$

These coefficients are computed at a renormalisation scale fixed to the centre-of-mass energy, and depend therefore only on the value of the observable y. They explicitly include only QCD corrections with non-singlet quark couplings and are therefore independent of electroweak couplings. At $\mathcal{O}(\alpha_s^2)$, these amount to the full corrections, while the $\mathcal{O}(\alpha_s^3)$ corrections also receive a pure-singlet contribution. This pure-singlet contribution arises from the interference of diagrams where the external gauge boson couples to different quark lines. In four-jet observables at $\mathcal{O}(\alpha_s^3)$, these singlet contributions were found to be extremely small [24]. Also, the pure-singlet contribution from three-gluon final states to three-jet observables was found to be negligible [25]. This small correction to NNLO is denoted by δ_C:

$$\left.\frac{1}{\sigma_0}\frac{\mathrm{d}\sigma}{\mathrm{d}y}\right|_{\text{NNLO, pure singlet}} = \left(\frac{\alpha_s}{2\pi}\right)^3 \frac{\mathrm{d}\delta_C}{\mathrm{d}y}(s, M_Z, \alpha, \sin^2\Theta_W, c_q) \tag{3.8}$$

where c_q denotes the set of all electroweak vector and axial-vector quark couplings.

First-order electroweak corrections to event shape observables could be of a magnitude comparable to the NNLO QCD corrections. Like the pure-singlet NNLO contributions, these do also not factorise onto σ_0. The first-order electroweak corrections affect the distribution itself and the normalisation σ_{had}. Collectively, they give a contribution of the form,

$$\left.\frac{1}{\sigma_{\text{had}}}\frac{\mathrm{d}\sigma}{\mathrm{d}y}\right|_{\text{electroweak},\mathcal{O}(\alpha\alpha_s)} = \left(\frac{\alpha}{2\pi}\right)\left(\frac{\alpha_s}{2\pi}\right)\frac{\mathrm{d}\delta_{EW}}{\mathrm{d}y}(s, M_Z, \alpha, \sin^2\Theta_W, c_q). \tag{3.9}$$

These corrections are not complete at present [26], and clearly deserve further study.

In summary, the expression for event shape distributions accurate to NNLO in QCD and NLO in the electroweak theory reads:

$$\begin{aligned}\frac{1}{\sigma_{\text{had}}}\frac{\mathrm{d}\sigma}{\mathrm{d}y} = &\left(\frac{\alpha_s}{2\pi}\right)\frac{\mathrm{d}\bar{A}}{\mathrm{d}y} + \left(\frac{\alpha_s}{2\pi}\right)^2\frac{\mathrm{d}\bar{B}}{\mathrm{d}y} + \left(\frac{\alpha_s}{2\pi}\right)^3\frac{\mathrm{d}\bar{C}}{\mathrm{d}y}\\ &+ \left(\frac{\alpha_s}{2\pi}\right)^3\frac{\mathrm{d}\delta_C}{\mathrm{d}y}(s, M_Z, \alpha, \sin^2\Theta_W, c_q)\\ &+ \left(\frac{\alpha}{2\pi}\right)\left(\frac{\alpha_s}{2\pi}\right)\frac{\mathrm{d}\delta_{EW}}{\mathrm{d}y}(s, M_Z, M_H, \alpha, \sin^2\Theta_W, c_q)\,.\end{aligned} \tag{3.10}$$

In the following, we will focus on the QCD non-singlet expression (3.1), since δ_C can be safely neglected, and the computation of δ_{EW} needs further work.

The QCD coupling constant evolves according to the renormalisation group equation, which is to NNLO:

$$\mu^2\frac{\mathrm{d}\alpha_s(\mu)}{\mathrm{d}\mu^2} = -\alpha_s(\mu)\left[\beta_0\left(\frac{\alpha_s(\mu)}{2\pi}\right) + \beta_1\left(\frac{\alpha_s(\mu)}{2\pi}\right)^2 + \beta_2\left(\frac{\alpha_s(\mu)}{2\pi}\right)^3 + \mathcal{O}(\alpha_s^4)\right] \tag{3.11}$$

LO	$\gamma^* \to q\,\bar{q}g$	tree level
NLO	$\gamma^* \to q\,\bar{q}g$	one loop
	$\gamma^* \to q\,\bar{q}\,gg$	tree level
	$\gamma^* \to q\,\bar{q}\,q\bar{q}$	tree level
NNLO	$\gamma^* \to q\,\bar{q}g$	two loop
	$\gamma^* \to q\,\bar{q}\,gg$	one loop
	$\gamma^* \to q\,\bar{q}\,q\,\bar{q}$	one loop
	$\gamma^* \to q\,\bar{q}\,q\,\bar{q}\,g$	tree level
	$\gamma^* \to q\,\bar{q}\,g\,g\,g$	tree level

Table 1: Non-singlet partonic contributions to three-jet event shape observables in perturbative QCD.

with the $\overline{\text{MS}}$-scheme coefficients

$$\begin{aligned}
\beta_0 &= \frac{11C_A - 4T_R N_F}{6}\,, \\
\beta_1 &= \frac{17C_A^2 - 10C_A T_R N_F - 6C_F T_R N_F}{6}\,, \\
\beta_2 &= \frac{1}{432}(2857C_A^3 + 108C_F^2 T_R N_F - 1230C_F C_A T_R N_F - 2830C_A^2 T_R N_F \\
&\quad +264C_F T_R^2 N_F^2 + 316C_A T_R^2 N_F^2).
\end{aligned} \tag{3.12}$$

Equation (3.11) is solved by introducing Λ as integration constant with $L = \log(\mu^2/\Lambda^2)$, yielding the running coupling constant:

$$\alpha_s(\mu) = \frac{2\pi}{\beta_0 L}\left(1 - \frac{\beta_1}{\beta_0^2}\frac{\log L}{L} + \frac{1}{\beta_0^2 L^2}\left(\frac{\beta_1^2}{\beta_0^2}\left(\log^2 L - \log L - 1\right) + \frac{\beta_2}{\beta_0}\right)\right)\,. \tag{3.13}$$

In terms of the running coupling $\alpha_s(\mu)$, the NNLO (non-singlet) expression for event shape distributions becomes

$$\begin{aligned}
\frac{1}{\sigma_{\text{had}}}\frac{\mathrm{d}\sigma}{\mathrm{d}y}(s,\mu^2,y) &= \left(\frac{\alpha_s(\mu)}{2\pi}\right)\frac{\mathrm{d}\bar{A}}{\mathrm{d}y} + \left(\frac{\alpha_s(\mu)}{2\pi}\right)^2\left(\frac{\mathrm{d}\bar{B}}{\mathrm{d}y} + \frac{\mathrm{d}\bar{A}}{\mathrm{d}y}\beta_0\log\frac{\mu^2}{s}\right) \\
&\quad + \left(\frac{\alpha_s(\mu)}{2\pi}\right)^3\left(\frac{\mathrm{d}\bar{C}}{\mathrm{d}y} + 2\frac{\mathrm{d}\bar{B}}{\mathrm{d}y}\beta_0\log\frac{\mu^2}{s} + \frac{\mathrm{d}\bar{A}}{\mathrm{d}y}\left(\beta_0^2\log^2\frac{\mu^2}{s} + \beta_1\log\frac{\mu^2}{s}\right)\right) \\
&\quad + \mathcal{O}(\alpha_s^4)\,.
\end{aligned} \tag{3.14}$$

4. Calculation of NNLO corrections

Three-jet production at tree-level is induced by the decay of a virtual photon (or other neutral gauge boson) into a quark-antiquark-gluon final state. At higher orders, this process receives corrections from extra real or virtual particles. The individual partonic channels that contribute through to NNLO are shown in table 1. All of the tree-level and loop amplitudes associated with these channels are known in the literature [13, 27, 14, 15].

For a given partonic final state, the event shape observable y is computed according to the same definition as in the experiment, which is applied to partons instead of hadrons. At leading order, all three final state partons must be well separated from each other, such that y differs from the trivial two-parton limit. At NLO, up to four partons can be present in the final state, two of which can be clustered together, whereas at NNLO, the final state can consist of up to five partons, and as many as three partons can be clustered together. The more partons in the final state, the better one expects the matching between theory and experiment to be [28].

The two-loop $\gamma^* \to q\bar{q}g$ matrix elements were derived in [13] by reducing all relevant Feynman integrals to a small set of master integrals using integration-by-parts [29] and Lorentz invariance [30] identities, solved with the Laporta algorithm [31]. The master integrals [32] were computed from their differential equations [30] and expressed analytically in terms of one- and two-dimensional harmonic polylogarithms [33].

The one-loop four-parton matrix elements relevant here [14] were originally derived in the context of NLO corrections to four-jet production and related event shapes [34, 35]. One of these four-jet parton-level event generator programs [35] is the starting point for our calculation, since it already contains all relevant four-parton and five-parton matrix elements.

The four-parton and five-parton contributions to three-jet-like final states at NNLO contain infrared real radiation singularities, which have to be extracted and combined with the infrared singularities [36] present in the virtual three-parton and four-parton contributions to yield a finite result. In our case, this is accomplished by introducing subtraction functions, which account for the infrared real radiation singularities, and are sufficiently simple to be integrated analytically. Schematically, this subtraction reads:

$$\begin{aligned}
\mathrm{d}\sigma_{\mathrm{NNLO}} = & \int_{\mathrm{d}\Phi_5} \left(\mathrm{d}\sigma^{R}_{\mathrm{NNLO}} - \mathrm{d}\sigma^{S}_{\mathrm{NNLO}}\right) \\
& + \int_{\mathrm{d}\Phi_4} \left(\mathrm{d}\sigma^{V,1}_{\mathrm{NNLO}} - \mathrm{d}\sigma^{VS,1}_{\mathrm{NNLO}}\right) \\
& + \int_{\mathrm{d}\Phi_5} \mathrm{d}\sigma^{S}_{\mathrm{NNLO}} + \int_{\mathrm{d}\Phi_4} \mathrm{d}\sigma^{VS,1}_{\mathrm{NNLO}} + \int_{\mathrm{d}\Phi_3} \mathrm{d}\sigma^{V,2}_{\mathrm{NNLO}} \,,
\end{aligned}$$

where $\mathrm{d}\sigma^{S}_{\mathrm{NNLO}}$ denotes the real radiation subtraction term coinciding with the five-parton tree level cross section $\mathrm{d}\sigma^{R}_{\mathrm{NNLO}}$ in all singular limits [37]. Likewise, $\mathrm{d}\sigma^{VS,1}_{\mathrm{NNLO}}$ is the one-loop virtual subtraction term coinciding with the one-loop four-parton cross section $\mathrm{d}\sigma^{V,1}_{\mathrm{NNLO}}$ in all singular limits [38]. Finally, the two-loop correction to the three-parton cross section is denoted by $\mathrm{d}\sigma^{V,2}_{\mathrm{NNLO}}$. With these, each line in the above equation is individually infrared finite, and can be integrated numerically.

Systematic methods to derive and integrate subtraction terms were available in the literature only to NLO [39, 40]. Physical results for the special case of NNLO Higgs production have been achieved in [41]. In the context of this project, we fully developed an NNLO subtraction formalism [42, 16, 17], based on the antenna subtraction method originally proposed at NLO [35, 40]. The basic idea of the antenna subtraction approach is to construct the subtraction terms from antenna functions. Each antenna function encap-

sulates all singular limits due to the emission of one or two unresolved partons between two colour-connected hard partons. This construction exploits the universal factorisation of phase space and squared matrix elements in all unresolved limits. The individual antenna functions are obtained by normalising three-parton and four-parton tree-level matrix elements and three-parton one-loop matrix elements to the corresponding two-parton tree-level matrix elements. Three different types of antenna functions are required, corresponding to the different pairs of hard partons forming the antenna: quark-antiquark, quark-gluon and gluon-gluon antenna functions. All these can be derived systematically from matrix elements [42] for physical processes.

The factorisation of the final state phase space into antenna phase space and hard phase space requires a mapping of the antenna momenta onto reduced hard momenta. We use the mapping derived in [43] for the three-parton and four-parton antenna functions. To extract the infrared poles of the subtraction terms, the antenna functions must be integrated analytically over the appropriate antenna phase spaces, which is done by reduction [44] to known phase space master integrals [45].

We tested the proper implementation of the subtraction by generating trajectories of phase space points approaching a given single or double unresolved limit. Along these trajectories, we observe that the antenna subtraction terms converge towards the physical matrix elements, and that the cancellations among individual contributions to the subtraction terms take place as expected. Moreover, we checked the correctness of the subtraction by introducing a lower cut (slicing parameter) on the phase space variables, and observing that our results are independent of this cut (provided it is chosen small enough). This behaviour indicates that the subtraction terms ensure that the contribution of potentially singular regions of the final state phase space does not contribute to the numerical integrals, but is accounted for analytically. A detailed description of the calculation can be found in [17].

The resulting numerical program, `EERAD3`, yields the full kinematical information on a given multi-parton final state. It can thus be used to compute any infrared-safe observable related to three-particle final states at $\mathcal{O}(\alpha_s^3)$ in e^+e^--annihilation.

5. NNLO distributions

In this section, we discuss the size and shape of the LO, NLO and NNLO coefficients of the perturbative expansion of the various event shape observables defined in eq. (3.6). For convenience, we weight the distribution by the observable.

The precise size and shape of the NNLO corrections depend on the observable in question. However, all contributions are dominated by the behaviour in the two-jet region where the observable generally tends to zero. Of course, typical hadronic events contain many hadrons and it is extremely unlikely that the value of any event shape is precisely zero for any experimental event. However, in the fixed order partonic calculation, where there are at most five partons present in the final state, one or more of the partons may be soft and/or collinear, and the observable may approach zero. In such circumstances, soft gluon singularities cause the fixed order prediction to become wildly unstable and grow

JHEP12(2007)094

logarithmically. In the infrared limit $y \to 0$, the perturbative coefficients have the following form,

$$\begin{aligned} y\frac{\mathrm{d}A}{\mathrm{d}y} &\sim A_1 L + A_0 \\ y\frac{\mathrm{d}B}{\mathrm{d}y} &\sim B_3 L^3 + B_2 L^2 + B_1 L + B_0 \\ y\frac{\mathrm{d}C}{\mathrm{d}y} &\sim C_5 L^5 + C_4 L^4 + C_3 L^3 + C_2 L^2 + C_1 L + C_0 \end{aligned} \tag{5.1}$$

where $L = \ln(1/y)$ and C_n are (as yet) undetermined coefficients. Whenever L is sufficiently large, resummation effects will be important. In our numerical studies, we therefore impose a cut on the size of y which is typically in the range 0.001–0.01, since for such small values of y we do not trust the fixed order prediction.

Even away from the infrared region, the shape of the fixed order prediction is heavily influenced by cancellations between the real and virtual contributions. The LO contribution A is very large and positive at small y and decreases monotonically as y increases. The NLO contribution B is negative at small y, but exhibits a turn-over, typically at $y \sim 0.05$. Similarly, the NNLO contribution C also exhibits a turn-over, but at a slightly larger value of y. The precise positions of the maxima of the distributions depend on the observable under consideration.

A second generic feature occurs when the paucity of final state particles imposes a maximum value for the observable. Examples include $(1-T)$ and C which are required to be less than 0.33 and 0.75 respectively for three-parton final states. As the number of partons increases with the perturbative order, this limit is relaxed and larger values of the observable are accessed.

Finally, typical values of the strong coupling constant lie around $\alpha_s \sim 0.12$, so that $\frac{\alpha_s}{2\pi} \sim 1/50$. It is well known that the NLO corrections are large, $B_y \sim (15-30)A_y$, leading to a 30-60% NLO effect in the region where the perturbative calculation is expected to be reliable. However, we observe that in all cases, the NNLO coefficients are also significant, $C_y \sim (200-800)A_y$, leading to a further 7-28% NNLO correction.

5.1 Thrust

Thrust is defined in section 2(a). First results for the NNLO corrections to the thrust distribution were presented in ref. [46]. The perturbative coefficients for the thrust distribution weighted by $(1-T)$ are shown in figure 1. As discussed earlier, the shape of the contribution is dominated by the infrared region at $(1-T) \to 0$. At small $(1-T)$, the LO contribution A is very large and positive, while the NLO and NNLO coefficients B and C are rising and exhibit a turn-over at moderate values of $(1-T)$. We observe that the peak moves from about 0.04 (NLO) to 0.06 (NNLO). We also see that the NLO and NNLO distributions progressively extend to larger and larger values of $(1-T)$ as the phase space restrictions on large values of $(1-T)$ are relaxed. In the intermediate region, $0.04 < (1-T) < 0.33$, we observe that the perturbative coefficients are roughly in the ratio, $A : B : C \sim 1 : 30 : 800$. Setting $\alpha_s \sim 0.12$ and using eq. (3.7), this indicates corrections

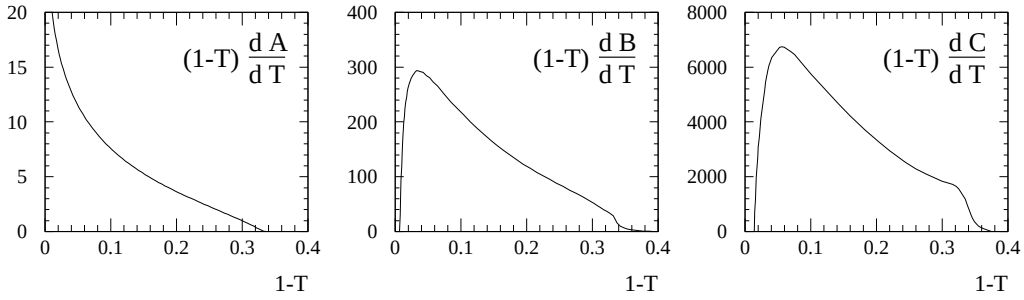

Figure 1: Coefficients of the leading order, next-to-leading order and next-to-next-to-leading order contributions to the thrust distribution as defined in eq. (3.6) and weighted by $(1-T)$.

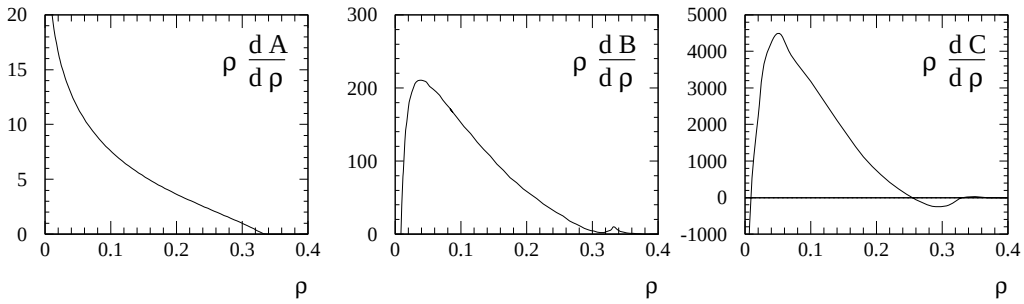

Figure 2: Coefficients of the leading order, next-to-leading order and next-to-next-to-leading order contributions to the heavy jet mass distribution as defined in eq. (3.6) and weighted by ρ.

which are of relative magnitude LO : NLO : NNLO $\sim 1 : 0.53 : 0.27$, such that the NNLO corrections increase the NLO prediction by another 18%.

5.2 Heavy jet mass

The definition of the heavy jet mass given in section 2(b) is the larger invariant mass of the two hemispheres formed by separating the event by a plane normal to the thrust axis. The perturbative coefficients for the heavy jet mass distribution weighted by ρ are shown in figure 2. At lowest order, the heavy jet mass and the $(1-T)$ distribution are identical, so that A does not extend past $\rho = 0.33$. At higher orders, the distribution extends to larger values, with a small negative NNLO contribution around 0.33. In the intermediate region, $0.02 < \rho < 0.33$, the perturbative coefficients are roughly $A : B : C \sim 1 : 20 : 400$ indicating corrections of approximately LO : NLO : NNLO $\sim 1 : 0.34 : 0.13$, translating into a 10% enhancement of NNLO over NLO. Comparing figure 1(b) with 2(b) and figure 1(c) with 2(c) we see clearly the rather different behaviour of the higher order corrections to these observables, particularly in the region beyond the LO kinematic bound where partonic configurations with two or more partons in each hemisphere contribute differently to each observable.

JHEP12(2007)094

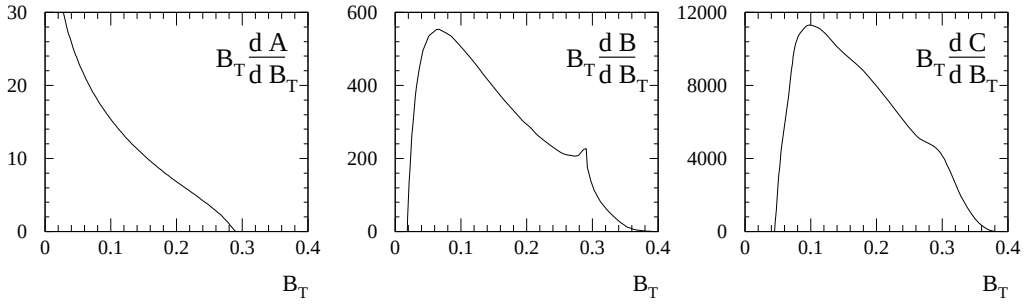

Figure 3: Coefficients of the leading order, next-to-leading order and next-to-next-to-leading order contributions to the total jet broadening distribution as defined in eq. (3.6) and weighted by B_T.

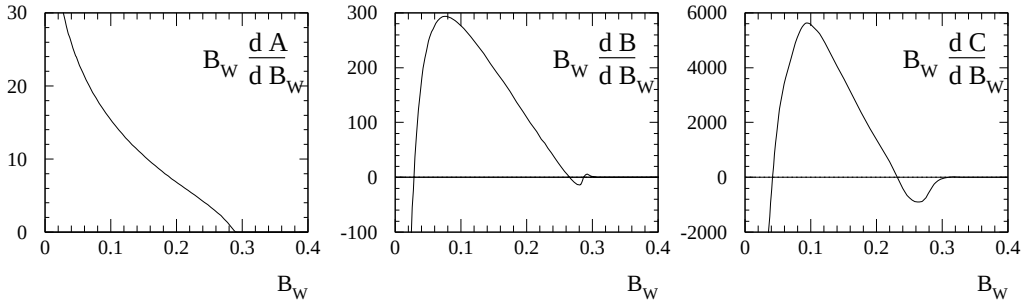

Figure 4: Coefficients of the leading order, next-to-leading order and next-to-next-to-leading order contributions to the wide jet broadening distribution as defined in eq. (3.6) and weighted by B_W.

5.3 Jet broadenings

The jet broadenings are defined in section 2(c) by dividing the event into two hemispheres using a plane normal to the thrust axis.. At lowest order B_W and B_T are identical, but their distributions receive different higher order corrections from partonic configurations with two or more partons in each hemisphere.

The perturbative coefficients for the B_T (B_W) distributions weighted by B_T (B_W) are shown in figure 3 (figure 4) respectively. The structures evident around B_T, $B_W \sim (1/2\sqrt{3}) \sim 0.29$ are generated by four and five parton events and are therefore different for the two observables. For more moderate B_T values between 0.04 and 0.29, the perturbative coefficients are in the ratio $A : B : C \sim 1 : 35 : 800$. Including the factors of α_s, this leads to corrections LO : NLO : NNLO $\sim 1 : 0.63 : 0.27$ for $\alpha_s \sim 0.12$, which amounts to NNLO corrections of 17% of the NLO result. We observe that the corrections for B_W are considerably smaller than those for B_T, $A : B : C \sim 1 : 20 : 400$ or equivalently $LO : NLO : NNLO \sim 1 : 0.34 : 0.13$, which yields a 10% NNLO effect over NLO. When $B_T < 0.04$ ($B_W < 0.04$), infrared logarithms must be resummed to produce a meaningful result.

JHEP12(2007)094

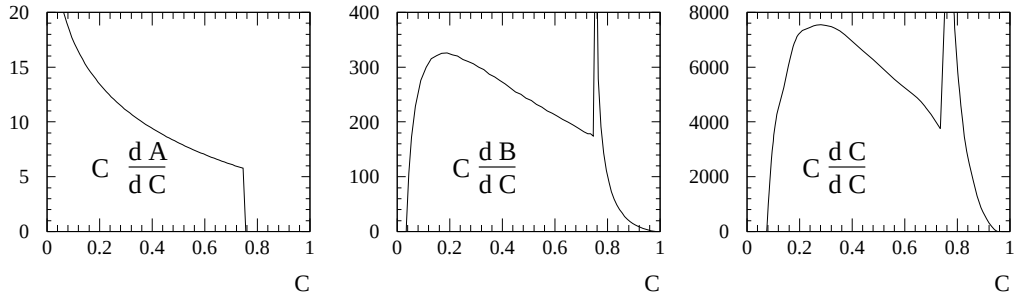

Figure 5: Coefficients of the leading order, next-to-leading order and next-to-next-to-leading order contributions to the C parameter distribution as defined in eq. (3.6) and weighted by C.

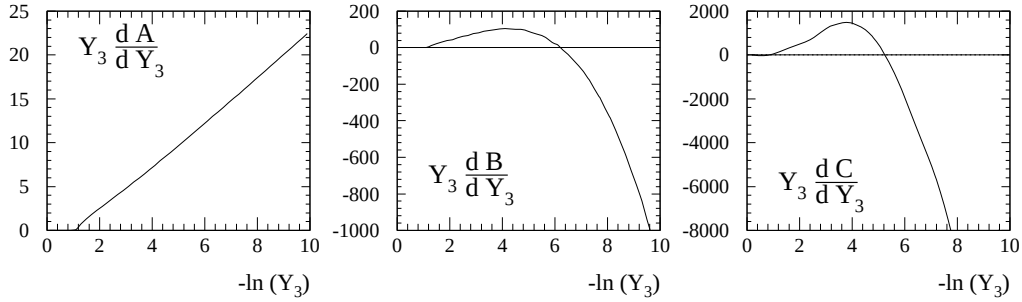

Figure 6: Coefficients of the leading order, next-to-leading order and next-to-next-to-leading order contributions to the distribution of the jet transition variable Y_3 as defined in eq. (3.6) and weighted by Y_3.

5.4 C-parameter

The C parameter is defined in section 2(d) and the perturbative distributions at LO, NLO and NNLO weighted by C are shown in figure 5. The LO kinematic limit at $C = 0.75$ is clearly visible. At NLO (and NNLO), four (and five) parton events can generate larger values of C, leading to a sharp peak around $C \sim 0.75$. The approximate size of the corrections for $0.1 < C < 0.75$ is $A : B : C \sim 1 : 30 : 700$, or, including the factors of $(\alpha_s/2\pi)$ with $\alpha_s \sim 0.12$, in the ratio LO : NLO : NNLO $\sim 1 : 0.53 : 0.23$, resulting in a 15% enhancement of NNLO over NLO. At smaller values of $C < 0.1$, large infrared logarithms render the fixed order prediction unreliable and must be resummed. Similarly, large logarithms are produced around the LO kinematic limit, $C \sim 0.75$ which must also be resummed.

5.5 Y_3

The jet transition variable Y_3 is defined in section 2(e). It describes the value of the jet resolution parameter $y_{\rm cut}$ for which an event changes from a three-jet to a two-jet configuration within the Durham jet algorithm. The perturbative distributions at LO, NLO and NNLO weighted by Y_3 are shown in figure 5. As with all of the event shapes, $Y_3 \mathrm{d}A/\mathrm{d}Y_3$ is linear when plotted on a logarithmic scale. For moderate values of Y_3, $2 < -\ln(Y_3) < 6$,

the corrections are positive. In this region, the approximate size of the corrections is $A : B : C \sim 1 : 15 : 200$, or, including the factors of $(\alpha_s/2\pi)$ with $\alpha_s \sim 0.12$, in the ratio LO : NLO : NNLO $\sim 1 : 0.25 : 0.06$, which produces a 5% NNLO effect over NLO. However, at smaller values of Y_3 (larger values of -ln(Y_3)) resummation of logarithmic contributions are clearly mandatory.

6. Comparison with data

We have presented the NNLO corrections to six event-shape distributions. As we have shown in the previous section, the magnitude of the NNLO correction is different for the six variables.

Each of the event shapes considered here has been studied in depth by all four experiments at LEP at centre-of-mass energies of 91.2, 133, 161, 172, 183, 189, 200 and 206 GeV [1 – 4]. Within the experimental uncertainties, these data sets are mutually consistent.

In this paper, we select data from ALEPH [1] as a representative set of hadronic final states in electron-positron annihilation to illustrate the improvement in the theoretical prediction due to the inclusion of the NNLO perturbative contribution. The only free parameter in our predictions is the strong coupling constant; we use the current world average value $\alpha_s(M_Z) = 0.1189$ [47].

The experimental event-shape distributions were computed using the reconstructed momenta and energies of charged and neutral particles. The measurements have been corrected for detector effects and the final distributions correspond to the particle (or hadron) level (stable hadrons and leptons after hadronisation). In addition, at LEP2 energies above the Z peak the data were corrected for initial-state radiation effects and backgrounds, mainly from W-pair production, were subtracted. The experimental uncertainties were estimated by varying event and particle selection cuts and are below 1% at LEP1 and between 0.5% and 1.5% at LEP2. For further details we refer the interested reader to ref. [1].

6.1 Thrust

Figure 7 displays the perturbative expression for the thrust distribution[2] at LO, NLO and NNLO, evaluated at $Q = M_Z$. The error band indicates the variation of the prediction under shifts of the renormalisation scale in the range $\mu \in [Q/2; 2\,Q]$ around the e^+e^- centre-of-mass energy Q. The relative scale uncertainty is reduced by about 30% between NLO and NNLO.

The inclusion of the NNLO corrections enhances the thrust distribution by around (15-20)% over the range $0.04 < (1-T) < 0.33$, where $-\ln(1-T)$ is not too large. Outside this range, one does not expect the perturbative fixed-order prediction to yield reliable results. For $(1-T) \to 0$, the convergence of the perturbative series is spoilt by powers

[2]First results for the NNLO corrections to the thrust distribution were presented in ref. [46].

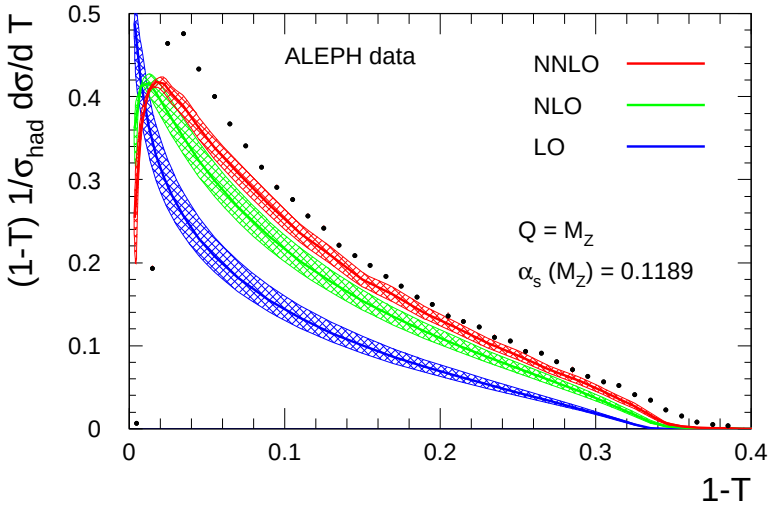

Figure 7: Thrust distribution at $Q = M_Z$ at LO (blue), NLO (green) and NNLO (red). The solid lines represent the prediction for renormalisation scale $\mu = Q$ and $\alpha_s(M_Z) = 0.1189$, while the shaded region shows the variation due to varying the renormalisation scale between $\mu = Q/2$ and $\mu = 2Q$. The data is taken from [1].

of logarithms $\ln(1 - T)$ appearing in higher perturbative orders, thus necessitating an all-order resummation of these logarithmic terms [10, 11], and a matching of fixed-order and resummed predictions [48].

The perturbative parton-level prediction is compared with the hadron-level data from the ALEPH collaboration [1] in figure 7 and figure 8. We observe that for all Q values, the shape and normalisation of the parton level NNLO prediction agrees better with the data than at NLO. We also see that the NNLO corrections account for approximately half of the difference between the parton-level NLO prediction and the hadron-level data.

6.2 Heavy jet mass

The perturbative prediction for the heavy jet mass distribution is displayed in figure 9. The solid lines represent the prediction at the physical scale $Q = M_Z$, while the shaded bands represent the effect of varying the renormalisation scale upwards and downwards by a factor of 2. We observe that the relative scale uncertainty is reduced by about 50% between NLO and NNLO. It is noteworthy that the original motivation for introducing the heavy jet mass distribution [20] was the hope for improved perturbative stability over the thrust distribution. This improved stability was not evident from the existing NLO results alone, but becomes visible at NNLO.

Compared to NLO, the inclusion of the NNLO corrections enhances the heavy jet mass distribution by around 10% over the range $0.02 < \rho < 0.33$, where $\ln(\rho)$ is not too large. At smaller ρ values, large $\ln(1/\rho)$ corrections must be resummed to all orders [49] and matched onto the perturbative prediction. Nevertheless, in the moderate to large ρ region, the NNLO corrections render the fixed order prediction significantly closer to the

JHEP12(2007)094

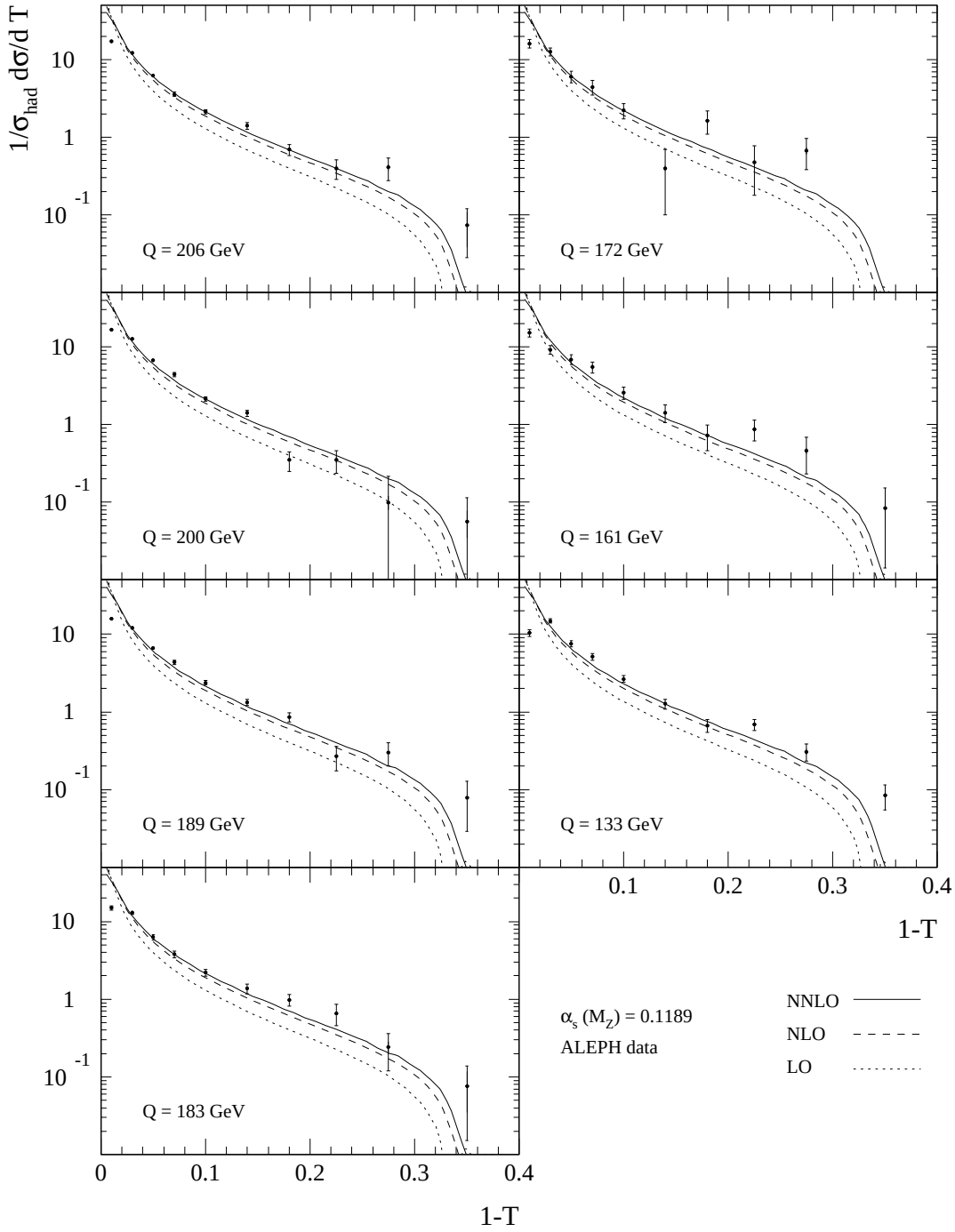

Figure 8: The thrust distribution (with $\mu = Q$ and $\alpha_s(M_Z) = 0.1189$) at LO (dotted), NLO (dashed) and NNLO (solid) compared to experimental data from ALEPH [1] for $Q = 133\,\text{GeV}, \ldots, 206\,\text{GeV}$.

experimental data [1].

Figure 10 shows the prediction for a range of Q values together with the hadron-level

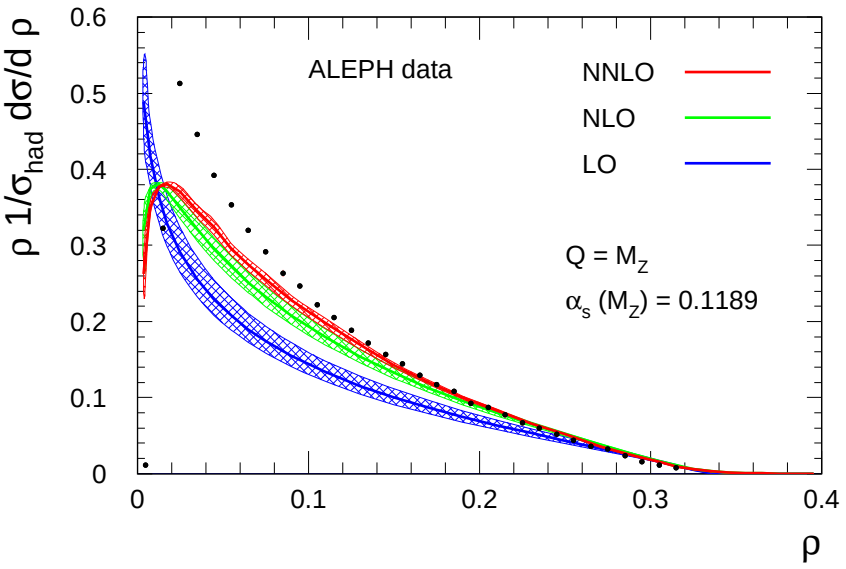

Figure 9: Heavy jet mass distribution at $Q = M_Z$ at LO (blue), NLO (green) and NNLO (red). The solid lines represent the prediction for renormalisation scale $\mu = Q$ and $\alpha_s(M_Z) = 0.1189$, while the shaded region shows the variation due to varying the renormalisation scale between $\mu = Q/2$ and $\mu = 2Q$. The data is taken from [1].

data from the ALEPH collaboration [1]. For this observable, the NNLO corrections are relatively small, however, for all Q values, the shape and normalisation of the parton-level NNLO prediction agrees slightly better with the hadron-level data than at NLO.

6.3 Jet broadenings

Predictions for the total and wide jet broadenings are displayed in figures 11 and 12. The solid lines represent the prediction at the physical scale $Q = M_Z$, while the shaded bands represent the effect of varying the renormalisation scale upwards and downwards by a factor of 2. We observe that the relative scale uncertainty in the B_T (B_W) distribution is reduced by about 40% (50%) between NLO and NNLO.

As anticipated from the discussion in section 5.3, we observe that the perturbative corrections are smaller for B_W than for B_T. In the region where perturbation theory is expected to yield reliable results, (B_T, B_W) > 0.05, we observe an enhancement of (15-20)% in B_T and of (8-12)% in B_W. As with $(1 - T)$ and the heavy jet mass, the two broadenings are identical at leading order, but display a largely different behaviour in the higher perturbative corrections. At smaller values of broadening, large logarithmic corrections occur which must be resummed [21].

To guide the eye, figures 11 and 12 also show hadron-level data from the ALEPH collaboration [1]. For both broadenings, we see that the NNLO prediction lies closer to the data, and, in fact, accounts for much of the difference between the NLO prediction and the hadron-level data.

JHEP12(2007)094

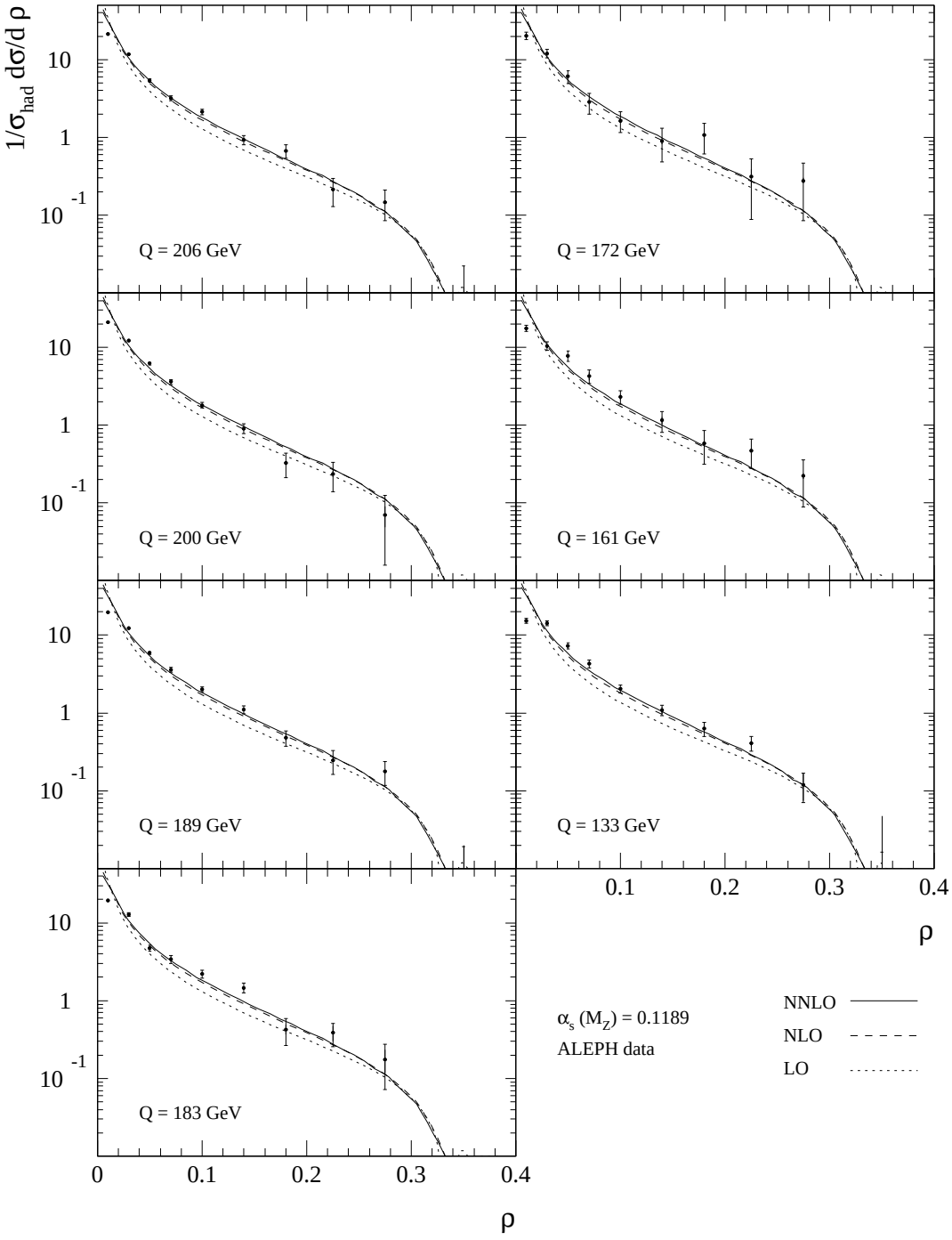

Figure 10: Heavy jet mass distribution (with $\mu = Q$ and $\alpha_s(M_Z) = 0.1189$) at LO (dotted), NLO (dashed) and NNLO (solid) compared to experimental data from ALEPH [1] for $Q = 133\ \text{GeV}, \ldots, 206\,\text{GeV}$.

The experiments at LEP also gathered data at higher Q values; figures 13 and 14 compare the parton-level prediction at $Q = 133\ \text{GeV}, \ldots, 206\,\text{GeV}$ with hadron-level data from

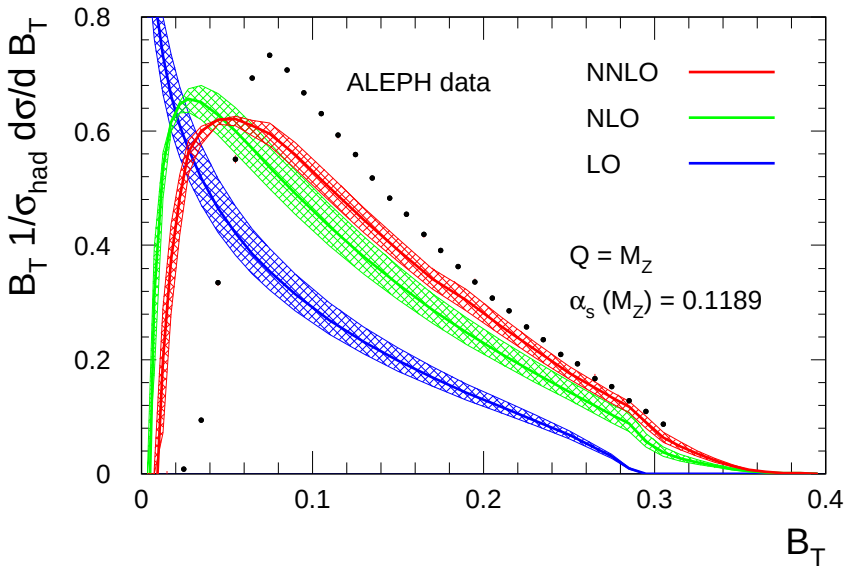

Figure 11: Total jet broadening distribution at $Q = M_Z$ at LO (blue), NLO (green) and NNLO (red). The solid lines represent the prediction for renormalisation scale $\mu = Q$ and $\alpha_s(M_Z) = 0.1189$, while the shaded region shows the variation due to varying the renormalisation scale between $\mu = Q/2$ and $\mu = 2Q$. The data is taken from [1].

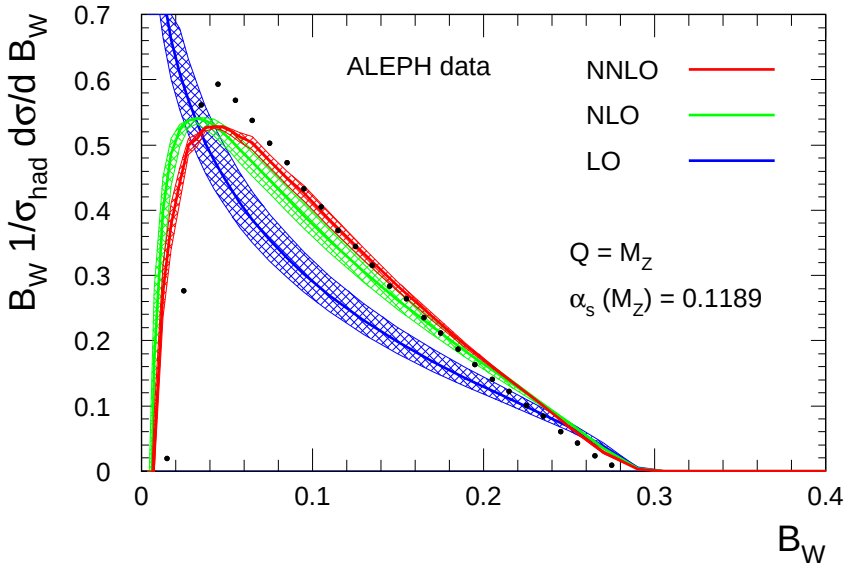

Figure 12: Wide jet broadening distribution at $Q = M_Z$ at LO (blue), NLO (green) and NNLO (red). The solid lines represent the prediction for renormalisation scale $\mu = Q$ and $\alpha_s(M_Z) = 0.1189$, while the shaded region shows the variation due to varying the renormalisation scale between $\mu = Q/2$ and $\mu = 2Q$. The data is taken from [1].

the ALEPH collaboration [1]. We observe that for all Q values, shape and normalisation of the parton level NNLO prediction agrees better with the data than at NLO.

JHEP12(2007)094

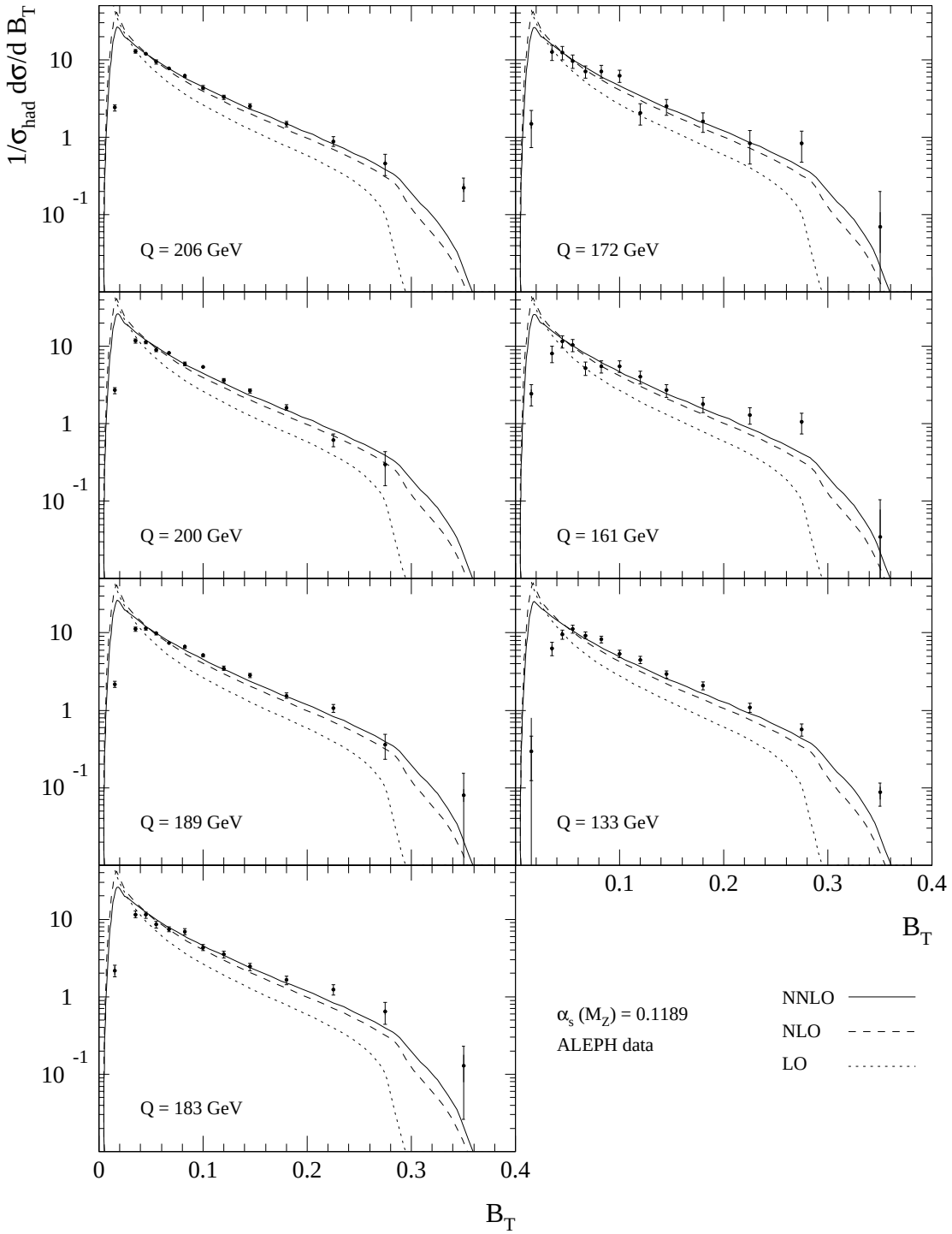

Figure 13: Total jet broadening distribution (with $\mu = Q$ and $\alpha_s(M_Z) = 0.1189$) at LO (dotted), NLO (dashed) and NNLO (solid) compared to experimental data from ALEPH [1] for $Q = 133\ \text{GeV}, \ldots, 206\,\text{GeV}$.

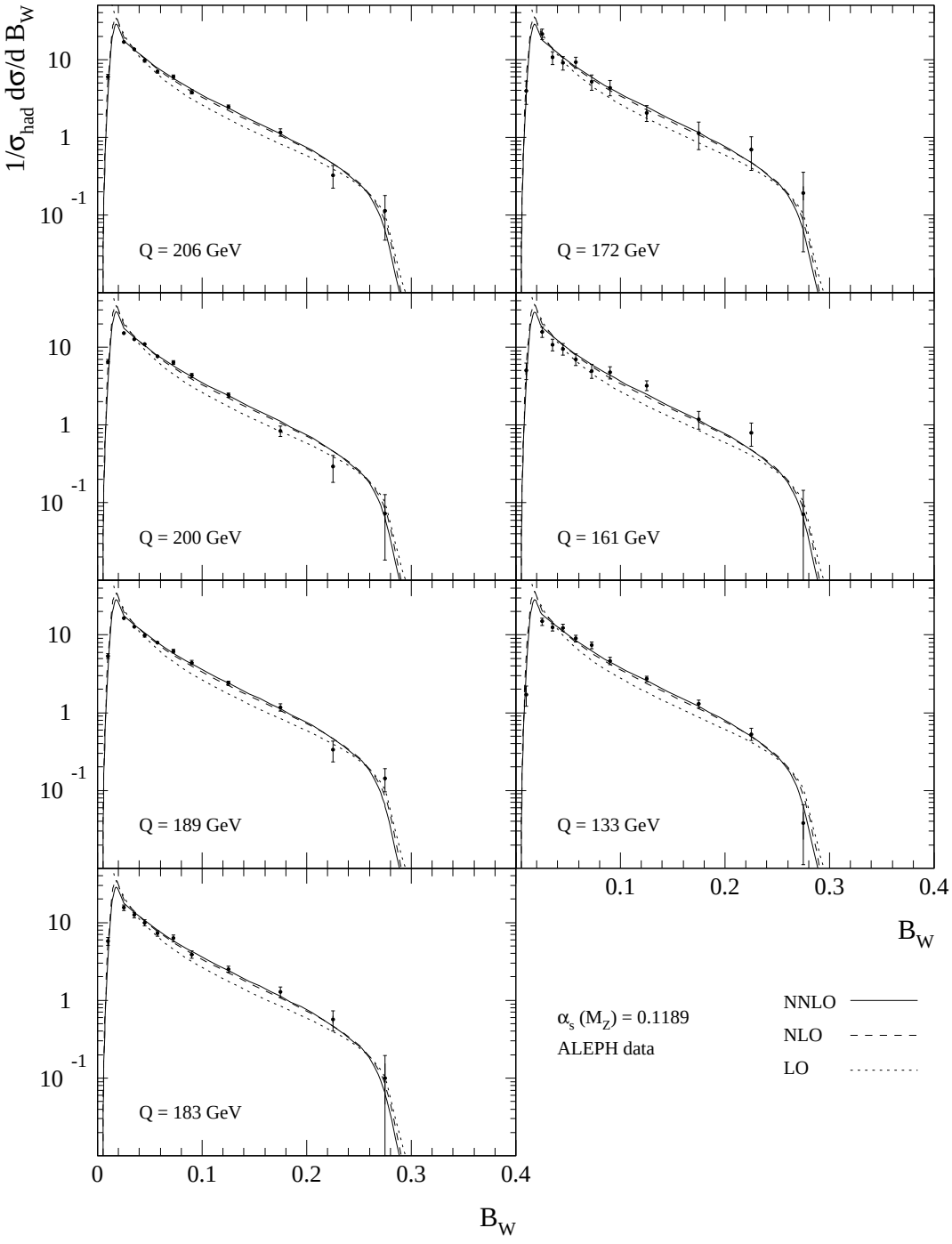

Figure 14: Wide jet broadening distribution (with $\mu = Q$ and $\alpha_s(M_Z) = 0.1189$) at LO (dotted), NLO (dashed) and NNLO (solid) compared to experimental data from ALEPH [1] for $Q = 133\,\text{GeV}, \ldots, 206\,\text{GeV}$.

6.4 C-parameter

The C parameter is one of the classic event shape observables and we display the pertur-

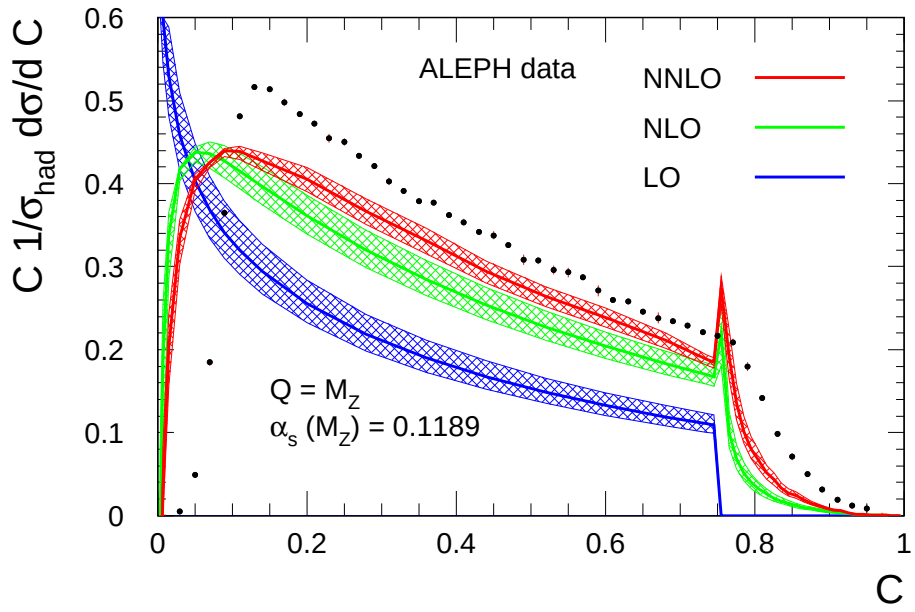

Figure 15: C parameter distribution at $Q = M_Z$ at LO (blue), NLO (green) and NNLO (red). The solid lines represent the prediction for renormalisation scale $\mu = Q$ and $\alpha_s(M_Z) = 0.1189$, while the shaded region shows the variation due to varying the renormalisation scale between $\mu = Q/2$ and $\mu = 2Q$. The data is taken from [1].

bative prediction in figure 15. The solid lines represent the prediction at the physical scale $Q = M_Z$, while the shaded bands represent the effect of varying the renormalisation scale upwards and downwards by a factor of 2. We observe that the relative scale uncertainty is reduced by about 40% between NLO and NNLO. The NNLO corrections enhance the C parameter distribution by around (12-20)% over the range $0.1 < C < 0.75$, where $\ln(1/C)$ is not too large. Figure 15 also shows hadron-level data from the ALEPH collaboration [1] and we observe that the NNLO parton-level prediction lies significantly closer to the data, and in fact, accounts for about one third of the difference between the NLO prediction and the data.

At small C, one expects large logarithmic contributions $\ln(1/C)$ appearing in higher perturbative orders, thus necessitating an all-order resummation of these logarithmic terms [50]. There are also large logarithms around $C \sim 0.75$, due to soft gluon divergences within the physical region (producing a so-called Sudakov shoulder in the distribution) which must also be resummed [51] to all orders.

Figure 16 shows the prediction for a range of Q values together with the hadron-level data from the ALEPH collaboration [1]. For all Q values, the shape and normalisation of the parton level NNLO prediction agrees slightly better with the data than at NLO.

6.5 Y_3

Figure 17 displays the perturbative expression for the Y_3 distribution at LO, NLO and NNLO, evaluated at $Q = M_Z$. The error band indicates the variation of the prediction

JHEP12(2007)094

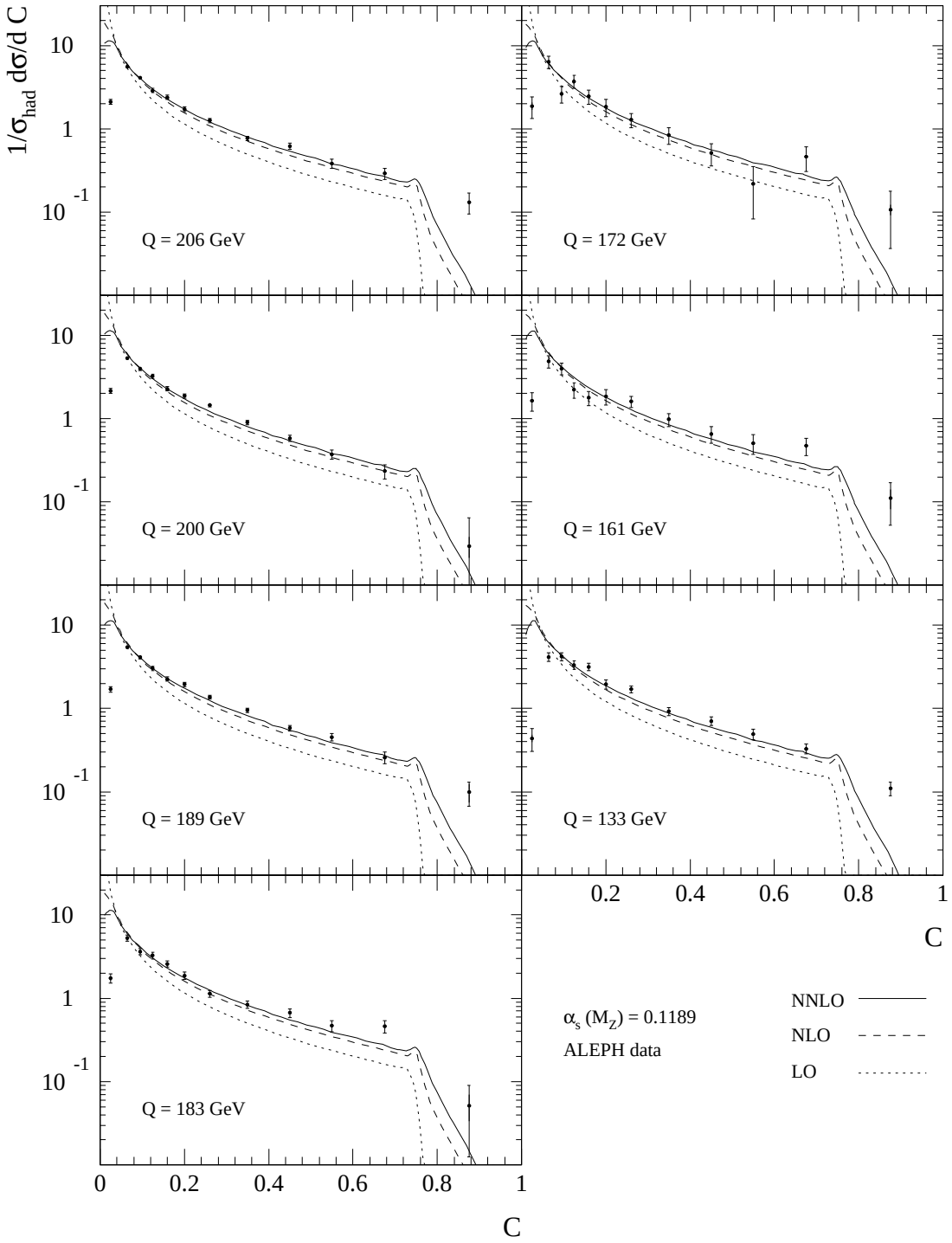

Figure 16: C parameter distribution (with $\mu = Q$ and $\alpha_s(M_Z) = 0.1189$) at LO (dotted), NLO (dashed) and NNLO (solid) compared to experimental data from ALEPH [1] for $Q = 133\,\text{GeV}, \ldots, 206\,\text{GeV}$.

JHEP12(2007)094

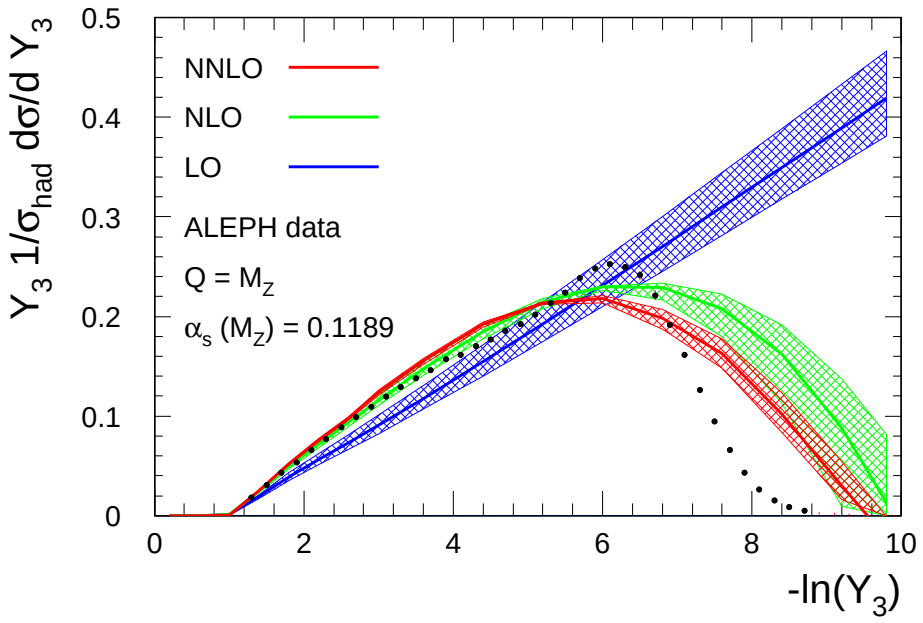

Figure 17: The distribution for the jet transition variable, Y_3 at $Q = M_Z$ at LO (blue), NLO (green) and NNLO (red). The solid lines represent the prediction for renormalisation scale $\mu = Q$ and $\alpha_s(M_Z) = 0.1189$, while the shaded region shows the variation due to varying the renormalisation scale between $\mu = Q/2$ and $\mu = 2Q$. The data is taken from [1].

under shifts of the renormalisation scale in the range $\mu \in [Q/2; 2\,Q]$ around the e^+e^- centre-of-mass energy Q. The relative scale uncertainty is reduced by about 50% between NLO and NNLO.

The NLO and NNLO corrections change the shape of the distribution considerably and introduce a turnover at $-\ln(Y_3) \sim 5 - 6$. We observe that the NNLO corrections modify the Y_3 distribution by around (3-5)% over the range $2 < -\ln(Y_3) < 6$, where $-\ln(Y_3)$ is moderate. At larger $-\ln(Y_3)$, one does not expect fixed-order perturbation theory to yield reliable results and the large infrared logarithms of the type $\alpha_s^n \ln^m(Y_3)$ must be resummed [52].

The perturbative parton-level prediction is compared with the hadron-level data from the ALEPH collaboration [1] in figure 17 and figure 18. We see that the quality of the agreement between fixed order perturbation theory and data is much more Q dependent than for the other observables considered in this paper. At $Q = M_Z$, the data is much more sharply peaked than the NNLO prediction. However, at higher Q values shown in figure 18, the agreement between the NNLO prediction and the data around the peak region is very good - and significantly better than at NLO.

7. Conclusions and outlook

The main goal of this paper is to provide improved theoretical predictions for hadronic event shape observables in electron-positron annihilation. To this end, we have presented

JHEP12(2007)094

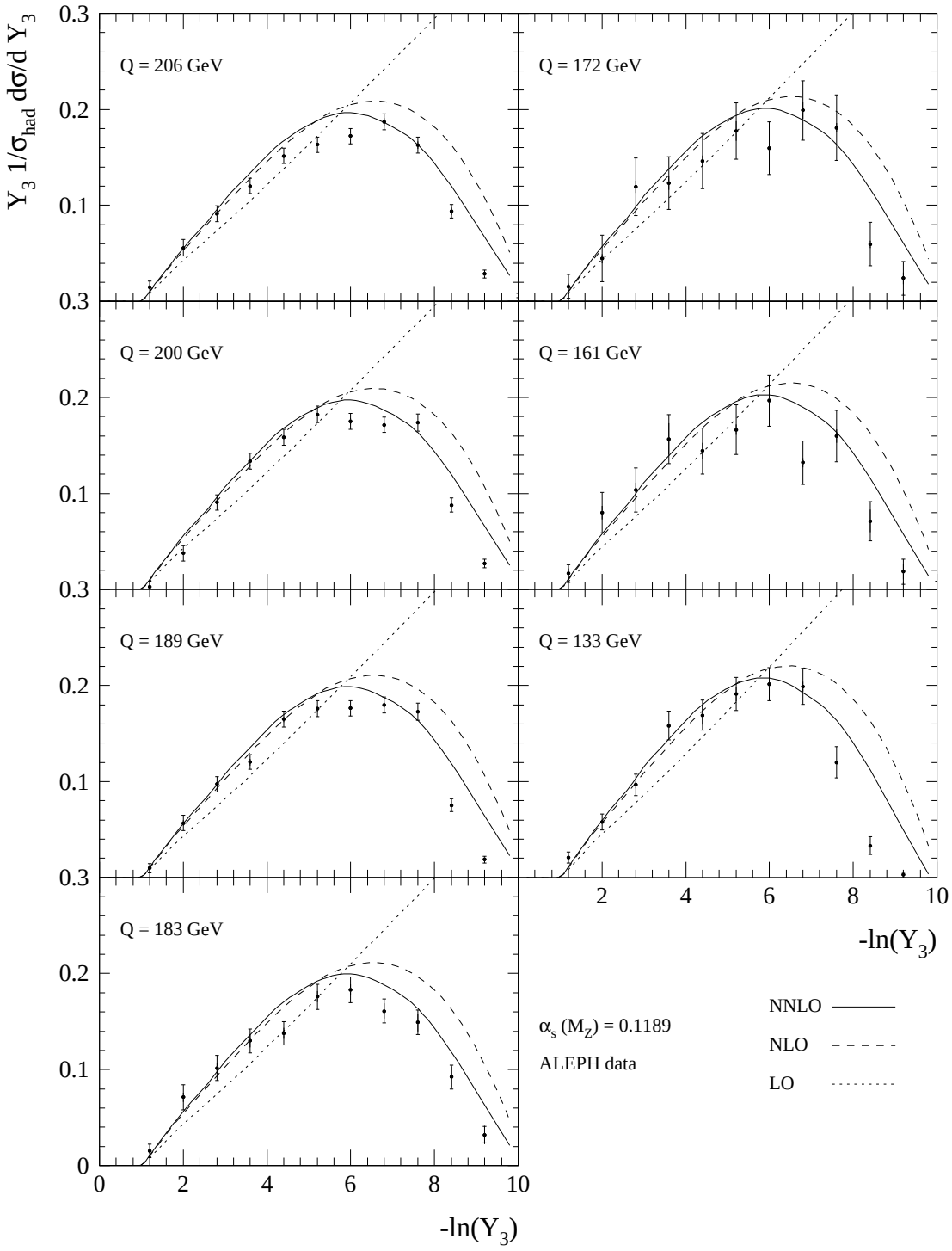

Figure 18: The Y_3 distribution (with $\mu = Q$ and $\alpha_s(M_Z) = 0.1189$) at LO (dotted), NLO (dashed) and NNLO (solid) compared to experimental data from ALEPH [1] for $Q = 133\ \text{GeV}, \ldots, 206\ \text{GeV}$.

new results for the next-to-next-to-leading order contributions to a number of important three-jet-like event shape observables in e^+e^- collisions. These results are obtained using a numerical program, that is based on the matrix elements for $\gamma^* \to 3$ partons at two-loop, $\gamma^* \to 4$ partons at one-loop and $\gamma^* \to 5$ partons at tree-level. Each of these contributions becomes singular when one or more partons are soft and/or collinear, and we have developed and implemented an NNLO subtraction formalism to subtract these singularities, thereby yielding a finite NNLO prediction. The resulting numerical program, `EERAD3`, yields the full kinematical information on the partonic final state and can be applied to generic infrared safe three-jet observables.

For the six event shapes considered here, and in kinematical regions where infrared logarithms are small enough to render their resummation unnecessary, the NLO corrections are generally large - of the order 30-60%. The NNLO effects produce a further 5-20% correction. Comparisons with existing data from LEP indicate an improved agreement with hadronic data and the fixed order NNLO parton-level prediction. In addition, the remaining theoretical uncertainty estimated by varying the renormalisation scale by a factor of two around the physical scale is also significantly reduced, typically by 30-50%. Importantly, the size of the corrections is different for different observables.

Our results for the NNLO corrections open up a whole new range of possible comparisons with the LEP data. For meaningful comparisons, one has to account for hadronisation effects, either by introducing hadron-level to parton-level correction factors, or by including power-suppressed hadronisation effects in the theoretical description. A first direct determination of the strong coupling constant from a fit of next-to-next-to-leading order QCD predictions to event-shape variables over a range of Q values will be reported in a separate publication [53] and should yield a much more precise value of $\alpha_s(M_Z)$ than that previously extracted from event shapes. Our predictions can be further improved by a NLL resummation of the large infrared logarithms that are present as $y \to 0$. The ingredients for $\ln R$ matching to NNLO are available in [11]. Studies in this direction are in progress and should yield a further improvement on the measurement of $\alpha_s(M_Z)$. Similarly, our results will also allow a renewed study of power corrections, now matched to NNLO.

Acknowledgments

We would like to thank Günther Dissertori and Hasko Stenzel for sharing their expertise on QCD event shapes in many useful discussions.

Part of this work was carried out while the authors were attending the programme "Advancing Collider Physics: From Twistors to Monte Carlos" of the Galileo Galilei Institute for Theoretical Physics (GGI) in Florence. We thank the GGI for its hospitality and the Istituto Nazionale di Fisica Nucleare (INFN) for partial support.

This research was supported in part by the Swiss National Science Foundation (SNF) under contract 200020-117602, by the UK Science and Technology Facilities Council and by the European Commission's Marie-Curie Research Training Network under contract MRTN-CT-2006-035505 "Tools and Precision Calculations for Physics Discoveries at Colliders".

References

[1] ALEPH collaboration, D. Buskulic et al., *Studies of QCD in e^+e^- → hadrons at $E_{cm} = 130\,GeV$ and 136 GeV*, *Z. Physik* **C 73** (1997) 409;
ALEPH collaboration, A. Heister et al., *Studies of QCD at e^+e^- centre-of-mass energies between 91 GeV and 209 GeV*, *Eur. Phys. J.* **C 35** (2004) 457.

[2] DELPHI collaboration, P. Abreu et al., *Energy dependence of event shapes and of α_s at LEP2*, *Phys. Lett.* **B 456** (1999) 322;
DELPHI collaboration, J. Abdallah et al., *A study of the energy evolution of event shape distributions and their means with the delphi detector at LEP*, *Eur. Phys. J.* **C 29** (2003) 285 [hep-ex/0307048];
DELPHI collaboration, J. Abdallah et al., *The measurement of α_s from event shapes with the delphi detector at the highest LEP energies*, *Eur. Phys. J.* **C 37** (2004) 1 [hep-ex/0406011].

[3] L3 collaboration, M. Acciarri et al., *Study of the structure of hadronic events and determination of α_s at $\sqrt{s} = 130\,GeV$ and 136 GeV*, *Phys. Lett.* **B 371** (1996) 137; *QCD studies and determination of α_s in e^+e^- collisions at $\sqrt{s} = 161\,GeV$ and 172 GeV*, *Phys. Lett.* **B 404** (1997) 390; *QCD results from studies of hadronic events produced in e^+e^- annihilations at $\sqrt{s} = 183\,GeV$*, *Phys. Lett.* **B 444** (1998) 569;
L3 collaboration, P. Achard et al., *Determination of alpha$_s$ from hadronic event shapes in e^+e^- annihilation at $192\,GeV \le \sqrt{s} \le 208\,GeV$*, *Phys. Lett.* **B 536** (2002) 217 [hep-ex/0206052]; *Studies of hadronic event structure in e^+e^- annihilation from 30 GeV to 209 GeV with the L3 detector*, *Phys. Rept.* **399** (2004) 71 [hep-ex/0406049].

[4] OPAL collaboration, P.D. Acton et al., *A determination of $\alpha_s(M_Z)$ at LEP using resummed QCD calculations*, *Z. Physik* **C 59** (1993) 1;
OPAL collaboration, G. Alexander et al., *QCD studies with e^+e^- annihilation data at 130 GeV and 136 GeV*, *Z. Physik* **C 72** (1996) 191;
OPAL collaboration, K. Ackerstaff et al., *QCD studies with e^+e^- annihilation data at 161 GeV*, *Z. Physik* **C 75** (1997) 193;
OPAL collaboration, G. Abbiendi et al., *QCD studies with e^+e^- annihilation data at 172 GeV to 189 GeV*, *Eur. Phys. J.* **C 16** (2000) 185 [hep-ex/0002012]; *Measurement of event shape distributions and moments in e^+e^- → hadrons at 91 GeV–209 GeV and a determination of α_s*, *Eur. Phys. J.* **C 40** (2005) 287 [hep-ex/0503051].

[5] SLD collaboration, K. Abe et al., *Measurement of α_s (M_Z) from hadronic event observables at the Z0 resonance*, *Phys. Rev.* **D 51** (1995) 962 [hep-ex/9501003].

[6] O. Biebel, *Experimental tests of the strong interaction and its energy dependence in electron positron annihilation*, *Phys. Rept.* **340** (2001) 165;
S. Kluth, *Tests of quantum chromo dynamics at e^+e^- colliders*, *Rept. Prog. Phys.* **69** (2006) 1771.

[7] R.K. Ellis, D.A. Ross and A.E. Terrano, *The perturbative calculation of jet structure in e^+e^- annihilation*, *Nucl. Phys.* **B 178** (1981) 421.

[8] Z. Kunszt, *Comment on the $O(\alpha_s^2)$ corrections to jet production in e^+e^- annihilation*, *Phys. Lett.* **B 99** (1981) 429;
J.A.M. Vermaseren, K.J.F. Gaemers and S.J. Oldham, *Perturbative QCD calculation of jet cross-sections in e^+e^- annihilation*, *Nucl. Phys.* **B 187** (1981) 301;
K. Fabricius, I. Schmitt, G. Kramer and G. Schierholz, *Higher order perturbative QCD calculation of jet cross-sections in e^+e^- annihilation*, *Z. Physik* **C 11** (1981) 315.

JHEP12(2007)094

[9] W.T. Giele and E.W.N. Glover, *Higher order corrections to jet cross-sections in e^+e^- annihilation*, *Phys. Rev.* **D 46** (1992) 1980;
S. Catani and M.H. Seymour, *The dipole formalism for the calculation of QCD jet cross sections at next-to-leading order*, *Phys. Lett.* **B 378** (1996) 287 [hep-ph/9602277].

[10] S. Catani, G. Turnock, B.R. Webber and L. Trentadue, *Thrust distribution in e^+e^- annihilation*, *Phys. Lett.* **B 263** (1991) 491.

[11] S. Catani, L. Trentadue, G. Turnock and B.R. Webber, *Resummation of large logarithms in e^+e^- event shape distributions*, *Nucl. Phys.* **B 407** (1993) 3.

[12] G.P. Korchemsky and G. Sterman, *Nonperturbative corrections in resummed cross-sections*, *Nucl. Phys.* **B 437** (1995) 415 [hep-ph/9411211];
Y.L. Dokshitzer and B.R. Webber, *Calculation of power corrections to hadronic event shapes*, *Phys. Lett.* **B 352** (1995) 451 [hep-ph/9504219]; *Power corrections to event shape distributions*, *Phys. Lett.* **B 404** (1997) 321 [hep-ph/9704298];
Y.L. Dokshitzer, A. Lucenti, G. Marchesini and G.P. Salam, *On the universality of the Milan factor for $1/q$ power corrections to jet shapes*, *JHEP* **05** (1998) 003 [hep-ph/9802381].

[13] L.W. Garland, T. Gehrmann, E.W.N. Glover, A. Koukoutsakis and E. Remiddi, *The two-loop QCD matrix element for $e^+e^- \to 3$-jets*, *Nucl. Phys.* **B 627** (2002) 107 [hep-ph/0112081]; *Two-loop QCD helicity amplitudes for $e^+e^- \to 3$-jets*, *Nucl. Phys.* **B 642** (2002) 227 [hep-ph/0206067].

[14] E.W.N. Glover and D.J. Miller, *The one-loop QCD corrections for $\gamma^* \to q\bar{q}q\bar{q}$*, *Phys. Lett.* **B 396** (1997) 257 [hep-ph/9609474];
Z. Bern, L.J. Dixon, D.A. Kosower and S. Weinzierl, *One-loop amplitudes for $e^+e^- \to \bar{q}qq\bar{q}$*, *Nucl. Phys.* **B 489** (1997) 3 [hep-ph/9610370];
J.M. Campbell, E.W.N. Glover and D.J. Miller, *The one-loop QCD corrections for $\gamma^* \to q\bar{q}gg$*, *Phys. Lett.* **B 409** (1997) 503 [hep-ph/9706297];
Z. Bern, L.J. Dixon and D.A. Kosower, *One-loop amplitudes for e^+e^- to four partons*, *Nucl. Phys.* **B 513** (1998) 3 [hep-ph/9708239].

[15] K. Hagiwara and D. Zeppenfeld, *Amplitudes for multiparton processes involving a current at e^+e^-, $e^\pm p$ and hadron colliders*, *Nucl. Phys.* **B 313** (1989) 560;
F.A. Berends, W.T. Giele and H. Kuijf, *Exact expressions for processes involving a vector boson and up to five partons*, *Nucl. Phys.* **B 321** (1989) 39;
N.K. Falck, D. Graudenz and G. Kramer, *Cross-section for five jet production in e^+e^- annihilation*, *Nucl. Phys.* **B 328** (1989) 317.

[16] A. Gehrmann-De Ridder, T. Gehrmann and E.W.N. Glover, *Antenna subtraction at NNLO*, *JHEP* **09** (2005) 056 [hep-ph/0505111]; *Quark-gluon antenna functions from neutralino decay*, *Phys. Lett.* **B 612** (2005) 36 [hep-ph/0501291]; *Gluon gluon antenna functions from Higgs boson decay*, *Phys. Lett.* **B 612** (2005) 49 [hep-ph/0502110].

[17] A. Gehrmann-De Ridder, T. Gehrmann, E.W.N. Glover and G. Heinrich, *Infrared structure of $e^+e^- \to 3$ jets at NNLO*, *JHEP* **11** (2007) 058 [arXiv:0710.0346].

[18] R.K. Ellis, W.J. Stirling and B.R. Webber, *QCD and collider physics*, Cambridge University Press, Cambridge U.K. (1996);
G. Dissertori, I.G. Knowles and M. Schmelling, *Quantum chromodynamics: high energy experiments and theory*, Oxford University Press (2003).

JHEP12(2007)094

[19] S. Brandt, C. Peyrou, R. Sosnowski and A. Wroblewski, *The principal axis of jets. an attempt to analyze high-energy collisions as two-body processes*, *Phys. Lett.* **A 12** (1964) 57;
E. Farhi, *A QCD test for jets*, *Phys. Rev. Lett.* **39** (1977) 1587.

[20] L. Clavelli and D. Wyler, *Kinematical bounds on jet variables and the heavy jet mass distribution*, *Phys. Lett.* **B 103** (1981) 383.

[21] P.E.L. Rakow and B.R. Webber, *Transverse momentum moments of hadron distributions in QCD jets*, *Nucl. Phys.* **B 191** (1981) 63;
S. Catani, G. Turnock and B.R. Webber, *Jet broadening measures in e^+e^- annihilation*, *Phys. Lett.* **B 295** (1992) 269.

[22] G. Parisi, *Super inclusive cross-sections*, *Phys. Lett.* **B 74** (1978) 65;
J.F. Donoghue, F.E. Low and S.-Y. Pi, *Tensor analysis of hadronic jets in quantum chromodynamics*, *Phys. Rev.* **D 20** (1979) 2759.

[23] S. Catani, Y.L. Dokshitzer, M. Olsson, G. Turnock and B.R. Webber, *New clustering algorithm for multi-jet cross-sections in e^+e^- annihilation*, *Phys. Lett.* **B 269** (1991) 432;
N. Brown and W.J. Stirling, *Jet cross-sections at leading double logarithm in e^+e^- annihilation*, *Phys. Lett.* **B 252** (1990) 657; *Finding jets and summing soft gluons: a new algorithm*, *Z. Physik* **C 53** (1992) 629;
W.J. Stirling et al., *Proceedings of the Durham workshop on jet physics at LEP and HERA*, *J. Phys.* **G 17** (1991) 1567;
S. Bethke, Z. Kunszt, D.E. Soper and W.J. Stirling, *New jet cluster algorithms: next-to-leading order QCD and hadronization corrections*, *Nucl. Phys.* **B 370** (1992) 310.

[24] A. Signer and L.J. Dixon, *Electron positron annihilation into four jets at next-to-leading order in α_s*, *Phys. Rev. Lett.* **78** (1997) 811 [hep-ph/9609460]; *Complete $O(\alpha_s^3)$ results for $e^+e^- \to (\gamma, Z) \to$ four jets*, *Phys. Rev.* **D 56** (1997) 4031 [hep-ph/9706285].

[25] J.J. van der Bij and E.W.N. Glover, *Z boson production and decay via gluons*, *Nucl. Phys.* **B 313** (1989) 237.

[26] E. Maina, S. Moretti and D.A. Ross, *Weak corrections to three-jet production in electron positron annihilations*, *JHEP* **04** (2003) 056 [hep-ph/0210015].

[27] S. Moch, P. Uwer and S. Weinzierl, *Two-loop amplitudes with nested sums: fermionic contributions to $e^+e^- \to q\bar{q}g$*, *Phys. Rev.* **D 66** (2002) 114001 [hep-ph/0207043].

[28] E.W.N. Glover, *Progress in NNLO calculations for scattering processes*, *Nucl. Phys.* **116** *(Proc. Suppl.)* (2003) 3 [hep-ph/0211412].

[29] F.V. Tkachov, *A theorem on analytical calculability of four loop renormalization group functions*, *Phys. Lett.* **B 100** (1981) 65;
K.G. Chetyrkin and F.V. Tkachov, *Integration by parts: the algorithm to calculate beta functions in 4 loops*, *Nucl. Phys.* **B 92** (1981) 159.

[30] T. Gehrmann and E. Remiddi, *Differential equations for two-loop four-point functions*, *Nucl. Phys.* **B 580** (2000) 485 [hep-ph/9912329].

[31] S. Laporta, *High-precision calculation of multi-loop Feynman integrals by difference equations*, *Int. J. Mod. Phys.* **A 15** (2000) 5087 [hep-ph/0102033].

[32] T. Gehrmann and E. Remiddi, *Two-loop master integrals for $\gamma^* \to 3$-jets: the planar topologies*, *Nucl. Phys.* **B 601** (2001) 248 [hep-ph/0008287]; *Two-loop master integrals for $\gamma^* \to 3$-jets: the non-planar topologies*, *Nucl. Phys.* **B 601** (2001) 287 [hep-ph/0101124].

JHEP12(2007)094

[33] E. Remiddi and J.A.M. Vermaseren, *Harmonic polylogarithms*, *Int. J. Mod. Phys.* **A 15** (2000) 725 [hep-ph/9905237];
T. Gehrmann and E. Remiddi, *Numerical evaluation of harmonic polylogarithms*, *Comput. Phys. Commun.* **141** (2001) 296 [hep-ph/0107173]; *Numerical evaluation of two-dimensional harmonic polylogarithms*, *Comput. Phys. Commun.* **144** (2002) 200 [hep-ph/0111255];
D. Maitre, *HPL, a mathematica implementation of the harmonic polylogarithms*, *Comput. Phys. Commun.* **174** (2006) 222 [hep-ph/0507152].

[34] Z. Nagy and Z. Trócsányi, *Next-to-leading order calculation of four-jet shape variables*, *Phys. Rev. Lett.* **79** (1997) 3604 [hep-ph/9707309];
S. Weinzierl and D.A. Kosower, *QCD corrections to four-jet production and three-jet structure in e^+e^- annihilation*, *Phys. Rev.* **D 60** (1999) 054028 [hep-ph/9901277].

[35] J.M. Campbell, M.A. Cullen and E.W.N. Glover, *Four jet event shapes in electron positron annihilation*, *Eur. Phys. J.* **C 9** (1999) 245 [hep-ph/9809429].

[36] S. Catani, *The singular behaviour of QCD amplitudes at two-loop order*, *Phys. Lett.* **B 427** (1998) 161 [hep-ph/9802439];
G. Sterman and M.E. Tejeda-Yeomans, *Multi-loop amplitudes and resummation*, *Phys. Lett.* **B 552** (2003) 48 [hep-ph/0210130].

[37] A. Gehrmann-De Ridder and E.W.N. Glover, *A complete $O(\alpha\alpha_s)$ calculation of the photon +1 jet rate in e^+e^- annihilation*, *Nucl. Phys.* **B 517** (1998) 269 [hep-ph/9707224];
J.M. Campbell and E.W.N. Glover, *Double unresolved approximations to multiparton scattering amplitudes*, *Nucl. Phys.* **B 527** (1998) 264 [hep-ph/9710255];
F.A. Berends and W.T. Giele, *Multiple soft gluon radiation in parton processes*, *Nucl. Phys.* **B 313** (1989) 595;
V. Del Duca, A. Frizzo and F. Maltoni, *Factorization of tree QCD amplitudes in the high-energy limit and in the collinear limit*, *Nucl. Phys.* **B 568** (2000) 211 [hep-ph/9909464];
S. Catani and M. Grazzini, *Collinear factorization and splitting functions for next-to-next-to-leading order QCD calculations*, *Phys. Lett.* **B 446** (1999) 143 [hep-ph/9810389]; *Infrared factorization of tree level QCD amplitudes at the next-to-next-to-leading order and beyond*, *Nucl. Phys.* **B 570** (2000) 287 [hep-ph/9908523].

[38] Z. Bern, L.J. Dixon, D.C. Dunbar and D.A. Kosower, *One-loop N-point gauge theory amplitudes, unitarity and collinear limits*, *Nucl. Phys.* **B 425** (1994) 217 [hep-ph/9403226];
D.A. Kosower, *All-order collinear behavior in gauge theories*, *Nucl. Phys.* **B 552** (1999) 319 [hep-ph/9901201];
D.A. Kosower and P. Uwer, *One-loop splitting amplitudes in gauge theory*, *Nucl. Phys.* **B 563** (1999) 477 [hep-ph/9903515];
Z. Bern, V. Del Duca and C.R. Schmidt, *The infrared behavior of one-loop gluon amplitudes at next-to-next-to-leading order*, *Phys. Lett.* **B 445** (1998) 168 [hep-ph/9810409];
Z. Bern, V. Del Duca, W.B. Kilgore and C.R. Schmidt, *The infrared behavior of one-loop QCD amplitudes at next-to-next-to-leading order*, *Phys. Rev.* **D 60** (1999) 116001 [hep-ph/9903516];
S. Catani and M. Grazzini, *The soft-gluon current at one-loop order*, *Nucl. Phys.* **B 591** (2000) 435 [hep-ph/0007142].

[39] Z. Kunszt and D.E. Soper, *Calculation of jet cross-sections in hadron collisions at order α_s^3*, *Phys. Rev.* **D 46** (1992) 192;
S. Frixione, Z. Kunszt and A. Signer, *Three-jet cross sections to next-to-leading order*, *Nucl. Phys.* **B 467** (1996) 399 [hep-ph/9512328];

JHEP12(2007)094

S. Catani and M.H. Seymour, *A general algorithm for calculating jet cross sections in NLO QCD*, *Nucl. Phys.* **B 485** (1997) 291 [hep-ph/9605323];
Z. Nagy and Z. Trócsányi, *Calculation of QCD jet cross sections at next-to-leading order*, *Nucl. Phys.* **B 486** (1997) 189 [hep-ph/9610498].

[40] D.A. Kosower, *Antenna factorization of gauge-theory amplitudes*, *Phys. Rev.* **D 57** (1998) 5410 [hep-ph/9710213]; *Antenna factorization in strongly-ordered limits*, *Phys. Rev.* **D 71** (2005) 045016 [hep-ph/0311272];
A. Daleo, T. Gehrmann and D. Maitre, *Antenna subtraction with hadronic initial states*, *JHEP* **04** (2007) 016 [hep-ph/0612257].

[41] S. Catani and M. Grazzini, *An NNLO subtraction formalism in hadron collisions and its application to Higgs boson production at the LHC*, *Phys. Rev. Lett.* **98** (2007) 222002 [hep-ph/0703012].

[42] A. Gehrmann-De Ridder, T. Gehrmann and E.W.N. Glover, *Infrared structure of* $e^+e^- \to$ *2-jets at NNLO*, *Nucl. Phys.* **B 691** (2004) 195 [hep-ph/0403057].

[43] D.A. Kosower, *Multiple singular emission in gauge theories*, *Phys. Rev.* **D 67** (2003) 116003 [hep-ph/0212097].

[44] C. Anastasiou and K. Melnikov, *Higgs boson production at hadron colliders in NNLO QCD*, *Nucl. Phys.* **B 646** (2002) 220 [hep-ph/0207004];
C. Anastasiou, L.J. Dixon, K. Melnikov and F. Petriello, *High-precision QCD at hadron colliders: electroweak gauge boson rapidity distributions at NNLO*, *Phys. Rev.* **D 69** (2004) 094008 [hep-ph/0312266].

[45] A. Gehrmann-De Ridder, T. Gehrmann and G. Heinrich, *Four-particle phase space integrals in massless QCD*, *Nucl. Phys.* **B 682** (2004) 265 [hep-ph/0311276].

[46] A. Gehrmann-De Ridder, T. Gehrmann, E.W.N. Glover and G. Heinrich, *Second-order QCD corrections to the thrust distribution*, *Phys. Rev. Lett.* **99** (2007) 132002 [arXiv:0707.1285].

[47] S. Bethke, *Experimental tests of asymptotic freedom*, *Prog. Part. Nucl. Phys.* **58** (2007) 351 [hep-ex/0606035].

[48] R.W.L. Jones, M. Ford, G.P. Salam, H. Stenzel and D. Wicke, *Theoretical uncertainties on* α_s *from event-shape variables in* e^+e^- *annihilations*, *JHEP* **12** (2003) 007 [hep-ph/0312016].

[49] S. Catani, G. Turnock and B.R. Webber, *Heavy jet mass distribution in* e^+e^- *annihilation*, *Phys. Lett.* **B 272** (1991) 368;
E. Gardi and J. Rathsman, *The thrust and heavy-jet mass distributions in the two-jet region*, *Nucl. Phys.* **B 638** (2002) 243 [hep-ph/0201019].

[50] S. Catani and B.R. Webber, *Resummed C-parameter distribution in* e^+e^- *annihilation*, *Phys. Lett.* **B 427** (1998) 377 [hep-ph/9801350];
E. Gardi and L. Magnea, *The C parameter distribution in* e^+e^- *annihilation*, *JHEP* **08** (2003) 030 [hep-ph/0306094].

[51] S. Catani and B.R. Webber, *Infrared safe but infinite: soft-gluon divergences inside the physical region*, *JHEP* **10** (1997) 005 [hep-ph/9710333].

[52] A. Banfi, G.P. Salam and G. Zanderighi, *Semi-numerical resummation of event shapes*, *JHEP* **01** (2002) 018 [hep-ph/0112156].

[53] G. Dissertori et al., *First determination of the strong coupling constant using NNLO predictions for hadronic event shapes in* e^+e^- *annihilations*, arXiv:0712.0327.

JHEP12(2007)094